JOURNAL OF AGRICULTURAL AND FOOD CHEMISTRY

pubs.acs.org/JAFC Article

Multiomics Identification and Structural Dynamics of PeXyn1: A Novel GH11 Xylanase from *Pleurotus eryngii* for Substrate Utilization

Xiaohang Li, Xianfeng Du, Yan Zhang, Xia Gao, Xinyu Liu, Chenxiao Zhang, Chunhui Hu, Lili Xu, Yanjiao Zhang, Hailong Yu,* and Hao Yu*

Cite This: https://doi.org/10.1021/acs.jafc.6c05044 Read Online

ACCESS | Metrics & More | Article Recommendations | Supporting Information

ABSTRACT: The widely cultivated mushroom *Pleurotus eryngii* utilizes lignocellulosic biomass as a growth substrate, yet its xylanases remain poorly understood. Here, we identified PeXyn1, a novel cellulose-upregulated GH11 xylanase featuring a C-terminal carbohydrate-binding module (CBM1) domain, using integrated multiomics. Recombinant PeXyn1 exhibited an optimal pH of 4.5 and temperature of 50 °C, with remarkable stability across pH 4.5−7.5. Kinetic characterization yielded a *K*m of 27.51 mg mL^{-1} and a *k*cat of 20.95 s^{-1}. Purified PeXyn1 efficiently saccharified corncob, releasing 4.258 mg mL^{-1} reducing sugars after 2 h. Notably, CBM1 truncation increased specific activity from 10.04 ± 0.29 to 28.79 ± 2.23 U mg^{-1}, confirming the core's hydrolytic function while CBM1 mediates substrate anchoring. Simulations revealed an induced-fit mechanism with a high xylohexaose binding affinity (−11.7 kJ mol^{-1}). Multivalent interactions at the CBM1-catalytic interface restrict structural fluctuations, promoting a stable conformation. This work offers the first molecular insight into *P. eryngii* xylanases, highlighting PeXyn1 for agro-waste valorization.

KEYWORDS: *mushroom, lignocellulose degradation, hemicellulose, gene cloning and expression, xylanase*

1. INTRODUCTION

Lignocellulosic agricultural residues are generated in massive quantities worldwide, with an estimated annual production exceeding 180 billion tons.[1,2] Owing to its abundance, lignocellulose holds considerable potential as a sustainable alternative to nonrenewable resources.[3−5] The utilization of agroforestry residues as substrates for mushroom cultivation represents a commercially viable strategy for the efficient bioconversion and valorization of lignocellulose. Efficient utilization of lignocellulose is critical for optimal mushroom growth and yield.[6−8] However, the intrinsic recalcitrance and structural complexity of the lignocellulosic matrix render it highly resistant to enzymatic degradation. Lignocellulose is primarily composed of three components: cellulose, hemicellulose, and lignin. Among these, hemicellulose is considered the most accessible and easily utilized fraction; consequently, hemicellulose-rich raw materials, such as corncobs, are frequently incorporated into substrate formulations as readily available carbon sources for edible mushroom production. Hemicellulose is a heterogeneous polysaccharide composed of pentoses and hexoses,[9] among which xylan represents the most abundant fraction. Xylan typically consists of 100−1000 xylose residues forming a linear backbone of β-(1,4)-linked β-D-xylopyranosyl units, which can be substituted with glucuronic acid or arabinose to generate glucuronoxylans and arabinoxylans.[9] Despite its importance, the specific mechanisms underlying hemicellulose utilization in mushrooms, particularly in the widely cultivated species *Pleurotus eryngii*, remain largely uncharacterized.

Pleurotus species are typically cultivated on various agricultural residues, including corncobs, cottonseed hulls, wheat bran, and sawdust.[10−12] Beyond their nutritional value, *Pleurotus* species, particularly *P. eryngii*, have attracted considerable interest as functional foods because of their rich repertoire of bioactive compounds and associated health-promoting properties. Previous studies have demonstrated that *Pleurotus* mushrooms possess significant antioxidant potential and can be developed as value-added functional food products. Furthermore, *P. eryngii* is highly regarded for its structurally unique bioactive polysaccharides, which exhibit potent anti-inflammatory and antioxidant activities.[13−16] In addition to their organic bioactive components, *Pleurotus* mushrooms accumulate various mineral elements, and ICP-OES analyses have shown abundant essential elements (e.g., K, Ca, Mg, Fe, Zn, Cu) with generally low heavy metal levels, indicating their safety for consumption, while also revealing species- and strain-dependent differences in elemental accumulation.[17] *P. eryngii* is classified as a white-rot fungus, which has remarkable lignocellulose-degrading capacity. Its lignocellulose-degrading machinery is extraordinarily complex and relies on the coordinated action of multiple enzyme classes.[18−21] Carbohydrate-active enzymes (CAZymes) play a central role in plant cell wall deconstruction, providing essential carbon sources for fungal growth, development, and reproduction. Species within the *Pleurotus* genus exhibit distinct advantages over other edible mushrooms, notably high enzyme productivity, a broad spectrum of substrate utilization, low nutritional requirements,

Received: April 4, 2026
Revised: July 9, 2026
Accepted: July 13, 2026

and robust environmental adaptability.[22] Furthermore, various *Pleurotus* species secrete substantial levels of cellulases during vegetative growth, with *Pleurotus flabellatus* reported to exhibit a significantly higher cellulase activity than allied species.[23] *P. eryngii* employs substrate-dependent lignocellulose degradation strategies and elaborates specific extracellular enzyme repertoires to efficiently deconstruct diverse lignocellulosic materials. Recent proteomic and secretomic analyses have uncovered pronounced variations in the secretion profiles of cellulases, lignin-degrading enzymes, and proteases when *P. eryngii* is cultivated on different types of agricultural residues.[24] Recent multiomics and metabolomic studies have shown that *Pleurotus* biology is tightly regulated at the systems level, where both developmental processes and environmental or processing conditions can reshape metabolic networks and functional metabolite profiles, highlighting a coordinated link between substrate utilization and metabolic adaptation.[25,26]

Endo-β-1,4-xylanases specifically cleave the internal β-1,4-glycosidic linkages within the xylan backbone, a predominant constituent of hemicellulose, to yield xylooligosaccharides and xylose. Consequently, xylanases represent the pivotal hydrolases for the efficient degradation of hemicellulose. Xylanases are prominent members of the CAZymes repertoire and are primarily categorized into the GH10 and GH11 families.[18,27] GH10 xylanases generally exhibit higher molecular weights (>40 kDa) and adopt a canonical $(\alpha/\beta)8$ barrel fold, with the catalytic site located at the wider opening of the barrel structure.[28,29] In contrast, GH11 xylanases are typically smaller proteins (<30 kDa) characterized by a higher substrate specificity but limited activity toward highly substituted xylans. These enzymes usually possess 5−6 substrate-binding subsites, among which the −3, +2, and +3 subsites are capable of accommodating L-arabinosyl substitutions.[30] Moreover, GH10- and GH11-type xylanases have found extensive applications in food and feed processing, biofuel production, the pulp and paper industry, ethanol fermentation, xylitol manufacturing, and the biomedical field.[31,32]

Genomic analyses of the genus *Pleurotus* have demonstrated that these fungi harbor a comprehensive and diverse repertoire of lignocellulose-degrading enzyme families.[33] Specifically, Baldrian et al. reported that, in the presence of chromium, extracellular cellulase activity in *Pleurotus* species increased significantly, whereas the induction of xylanase activity was delayed.[34] Previously, Altaf et al. characterized crude xylanase preparations from *P. eryngii* culture filtrates and reported optimal activity at pH 4.5 and 60 °C, along with remarkable stability across a broad pH range (4.0−10.0).[35] However, to the best of our knowledge, no xylanase gene from *P. eryngii* has been cloned and molecularly characterized to date.

In the present study, a novel GH11 endo-1,4-β-xylanase gene, designated as *PeXyn1*, was identified in *P. eryngii* through an integrated transcriptomic and proteomic analysis. The corresponding gene was cloned and heterologously expressed in *Pichia pastoris* GS115 and *Escherichia coli* BL21; subsequently, the recombinant enzyme was purified for comprehensive biochemical and physicochemical characterization. The catalytic properties of the purified xylanase were evaluated to assess its potential for industrial applications. Notably, this study represents the first successful heterologous expression of a xylanase gene from *P. eryngii*, offering crucial insights into the molecular mechanisms underlying hemicellulose degradation within the genus *Pleurotus*.

2. MATERIALS AND METHODS

2.1. Chemicals and Strain

The *P. eryngii* strain (NCMCC No. 240004) used in this study was deposited in the Center of Mushroom Culture Collection (mushroomseed.cn). *E. coli* DH5α and BL21(DE3) competent cells were purchased from Sangon Biotech (Shanghai, China) and cultured in Luria−Bertani (LB) medium. *P. pastoris* GS115 competent cells were obtained from TransGen Biotech (Beijing, China) and cultivated in yeast extract−peptone−dextrose (YPD) medium. Corncob xylan and beechwood xylan were purchased from Shanghai Macklin Biochemical Co., Ltd. (Shanghai, China) and Shanghai Yuanye Bio-Technology Co., Ltd. (Shanghai, China), respectively. All other reagents used in this study were of analytical grade unless otherwise specified.

2.2. Enzyme Induction and Multiomics Analysis

To induce the expression of carbohydrate hydrolases, *P. eryngii* was initially grown in BSNM liquid medium at 25 °C and 125 rpm for 5 d to allow sufficient mycelial growth, after which 5 g L^{-1} cellulose or xylan was added as an inducer (Supporting Information, Text S1). The activities of cellulase and xylanase were detected as previously described.[36] Mycelial samples were harvested at 36 h for transcriptomic analysis, and the supernatant was collected at 48 h for comparative proteomic evaluation.

Protein was extracted from the supernatant using a method described previously.[37] Following extraction and peptide digestion, the samples were subjected to label-free liquid chromatography-tandem mass spectrometry (LC−MS/MS). The comprehensive protocols detailing protein extraction, LC−MS/MS data acquisition, and the subsequent bioinformatics pipelines—including functional annotation, subcellular localization, and network analysis—are provided in the Supporting Information (see Supporting Information, Text S2).

Total RNA was extracted using TRIzol reagent (Takara, Kusatsu, Japan) according to the manufacturer's instructions, with the detailed extraction procedure provided in Supporting Information, Text S3. The extracted RNA from the designated time points was subjected to high-throughput sequencing. The comprehensive procedures for library preparation, RNA sequencing, and bioinformatics analysis are detailed in the Supporting Information (see Supporting Information, Text S4).

To validate the RNA-seq data and assess the expression of key genes, reverse transcription was performed using HiScript III Q RT SuperMix for qPCR (+gDNA wiper) (Vazyme, Nanjing, China). Quantitative real-time PCR (RT-qPCR) was carried out in a total reaction volume of 15 μL using ChamQ Universal SYBR qPCR Master Mix (Vazyme) on a SLAN-96S (Hongshi Biotech, Shanghai, China). The cycle threshold (C_t) values were normalized to the expression of the *GAPDH* gene, and relative gene expression levels were calculated using the $2^{-\Delta\Delta Ct}$ method. Each sample was analyzed in biological triplicate. The primer sequences used for RT-qPCR are listed in Supporting Information, Table S1.

2.3. Sequence and Phylogenetic Analysis

Structural features of PeXyn1 were analyzed using InterPro (http://www.ebi.ac.uk/interpro/search/sequence/). Motif prediction and amino acid frequency analysis within the identified motifs were performed using the MEME suite (https://meme-suite.org/meme/tools/meme). Once the highly conserved regions of each protein were selected, a multiple sequence alignment was performed using the MAFFT v7.526 program, which implements the Fast Fourier Transform (FFT) to optimize protein alignments based on the physicochemical properties of amino acids.[38] The protein sequence of PeXyn1 from *P. eryngii*, together with 21 GH11 xylanase sequences from other fungal species, was subjected to phylogenetic analysis using the Maximum Likelihood (ML) method implemented in MEGA11. The Jones−Taylor−Thornton (JTT) amino acid substitution model was applied with all sites included, and branch

https://doi.org/10.1021/acs.jafc.6c05044
J. Agric. Food Chem. XXXX, XXX, XXX−XXX

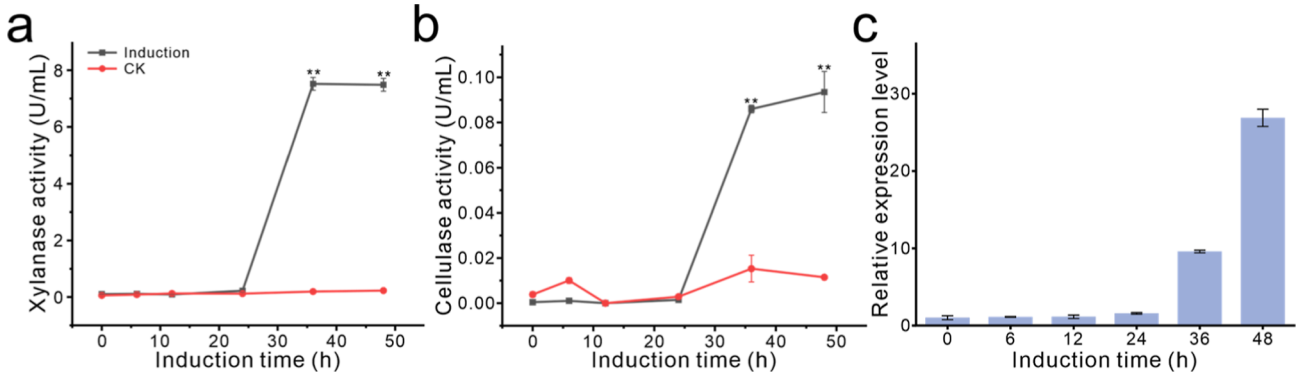

Figure 1. Patterns of enzyme activity expression in *P. eryngii* induced by cellulose powder. Xylanase (a) and cellulase (b) activity at different time points during cellulose induction. (c) Effects of cellulose induction on the expression levels of the xylanase *PeXyn1* gene.

support was assessed by 1000 bootstrap resamplings. The resulting consensus phylogenetic tree was visualized using FigTree v1.4.4.

2.4. Protein Expression and Purification

Total RNA was extracted from *P. eryngii* mycelial pellets as described above. First-strand cDNA was synthesized using the HiScript IV 1st Strand cDNA Synthesis Kit (+gDNA wiper) (Vazyme), following the manufacturer's instructions. Target fragments were subsequently amplified using gene-specific primers (Supporting Information, Table S2) and cloned into the respective expression vectors (pPIC9K for *P. pastoris* and pET-28a for *E. coli*) via homologous recombination. The pPIC9K-*PeXyn1* recombinant plasmid was linearized and subsequently transformed into *P. pastoris* GS115 by electroporation. Simultaneously, the pET-28a-*PeXyn1* plasmid was transformed into *E. coli* BL21(DE3) competent cells via heat shock. Induction conditions for both systems were optimized, and detailed protocols for strain construction and heterologous expression can be found in Supporting Information, Texts S5−S7. The expressed proteins were purified using Ni-NTA affinity chromatography. Molecular weight was assessed using 12% sodium dodecyl sulfate-polyacrylamide gel electrophoresis (SDS-PAGE).

2.5. Characterization and Kinetic Analysis of Recombinant PeXyn1

The pH-dependent activity range of recombinant PeXyn1 was measured at 25 °C across a pH range of 3.5−7.5. The effect of temperature on the activity of PeXyn1 was assessed within a temperature range of 25−80 °C. The thermal stability of PeXyn1 was evaluated by incubating the enzyme at 50 and 60 °C for 0−2 h under optimal pH conditions and measuring the residual activity. The Michaelis−Menten constant (K_m) and catalytic rate constant (k_{cat}) for PeXyn1 were determined using nonlinear regression analysis with the Michaelis−Menten model under optimal conditions (50 °C, pH 4.5). The enzyme activity of PeXyn1 was evaluated in the presence of 5 and 10 mM metal ions (Li^+, Mg^{2+}, K^+, Ca^{2+}, Mn^{2+}, Cu^{2+}, Zn^{2+}, and Cd^{2+}), and its substrate spectrum was determined. Additionally, the effects of various compounds and inhibitors (SDS, EDTA, methanol, acetone, and others) on enzyme activity were also assessed. The amino acid composition and elemental content of PeXyn1 were analyzed using the online ExPASy ProtParam tool.

2.6. Homology Modeling, Structural Prediction, and Molecular Docking

The three-dimensional structure of PeXyn1 was predicted using the AlphaFold Server (https://alphafoldserver.com).[39] AutoDock Vina was used for molecular docking simulations.[40] Xylo-oligosaccharides with degrees of polymerization (DP) of 2−6 were used as ligands. The structures of xylobiose to xylopentaose (CIDs: 439538, 52940105, 10230811, and 10146542) were retrieved from the PubChem database, while the structure of xylohexaose (X6) was extracted from the crystal structure of TrXyn11A (PDB ID: 4HK8).

The protein receptor and ligands were preprocessed using PyMOL version 3.1.6.1 (Schrödinger, LLC, New York, NY, USA) to remove water molecules, original ligands, and heteroatoms. AutoDockTools was used to prepare the input files by adding polar hydrogens, computing Gasteiger charges, and assigning AD4 atom types. The rotatable bonds of the ligands were defined, and a grid box was constructed to encompass the active site. Following docking with AutoDock Vina, the binding affinities between the protein and substrates were calculated. Postdocking interaction analysis and visualization were performed using Discovery Studio. Additionally, the pocket volume of the active site was calculated using the KVFinder-web service (https://kvfinder-web.cnpem.br/).

2.7. Molecular Dynamics Simulation

To evaluate the overall stability of the PeXyn1-substrate complex, molecular dynamics (MD) simulations were performed for 50 ns using the GROMACS software (version 2024.3) with the AMBER99SB force field. The system was solvated in a cubic box using the TIP3P water model, and appropriate counterions were added to neutralize the system charge. Energy minimization was carried out using the steepest descent algorithm until the maximum force on any atom was less than 1000 kJ mol^{-1} nm^{-1}. The bonds linked with hydrogen atoms were restrained with the LINCS algorithm. The temperature was maintained at 323 K using the *v*-rescale thermostat, while the pressure was kept at 1.0 bar using the Parrinello−Rahman barostat. The integration time step was set to 2 fs. Before the production runs, the system was equilibrated in the *NVT* ensemble for 100 ps, followed by another 100 ps of equilibration in the *NPT* ensemble. Subsequently, 50 ns production MD runs were conducted. Trajectory analyses, including root-mean-square deviation (RMSD), root-mean-square fluctuation (RMSF), radius of gyration (R_g), solvent-accessible surface area (SASA), and the number of hydrogen bonds, were performed using the built-in GROMACS utilities.

3. RESULTS AND DISCUSSION

3.1. A Novel Xylanase Was Identified in *P. eryngii* upon Cellulose Induction

In both natural ecosystems and artificial cultivation, the growth and development of mushrooms depend heavily on their capacity to depolymerize recalcitrant plant cell wall components. Lignocellulose-degrading enzymes are the essential core proteins driving these biological processes.[33] As one of the three principal constituents of lignocellulosic biomass, hemicellulose is primarily broken down by xylanases.[41] Given that most lignocellulose-degrading enzymes in edible fungi are induced by their corresponding polymer substrates or derivatives,[42,43] *P. eryngii* mycelia were cultivated in BSNM media to evaluate xylanase induction, with xylan and cellulose added as inducers at day 5. Subsequent enzyme assays demonstrated that cellulose significantly induced the produc-

https://doi.org/10.1021/acs.jafc.6c05044
J. Agric. Food Chem. XXXX, XXX, XXX−XXX

Table 1. Transcriptomic and Proteomic Analysis of Xylanase Induction by Cellulose Powder

			proteome		transcriptome	
ID	family	predicted protein function	CK	48 h	CK	36 h
KAF9492119	GH11	endo-1,4-beta-xylanase	0.074	94.499	4.143	274.344
KAF9492116	GH11	endo-1,4-beta-xylanase	0	20.994	24.673	251.995
KAF9501169	GH10	endo-1,4-beta-xylanase	0.497	13.983	6.505	346.990
KAF9489446	GH10	endo-1,4-beta-xylanase	0	3.923	5.945	242.998
KAF9489447	GH10	endo-1,4-beta-xylanase	0	2.359	9.611	223.318
KAF9489445	GH10	endo-1,4-beta-xylanase	0	0.071	12.616	15.139

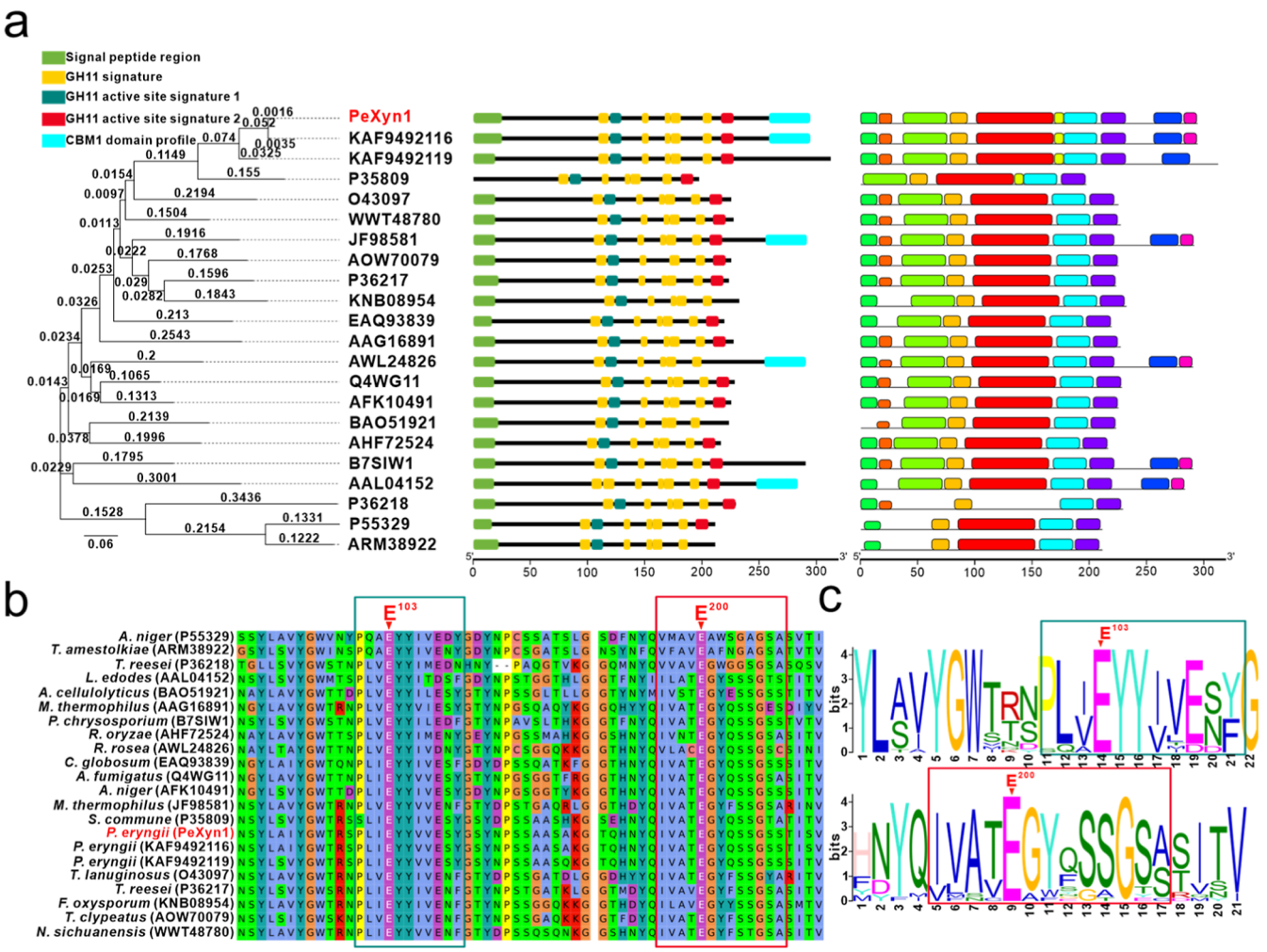

Figure 2. The phylogenetic and structural analyses of xylanase PeXyn1. (a) The phylogenetic tree aligned with domain architectures shows the distribution of conserved motifs and is consistent with the functional domain analysis (middle). (b) Alignment of GH11 active site signatures. The positions of the putative catalytic glutamate residues are highlighted. (c) Sequence logos depicting residue conservation flanking the active sites.

tion of both cellulase and xylanase. Specifically, upon cellulose induction, cellulase activity reached a 1311.29-fold (5.89 U mL^{-1}) increase compared to the control group after 10 d, while xylanase activity was upregulated by 15.10-fold in response to cellulose. Xylanase activity was 0.81- and 1.82-fold compared to control in response to xylan induction after 10 and 12 d, respectively (Figure S1). This phenomenon, in which cellulose acts as a stronger inducer of xylanase activity than xylan itself, likely reflects a coordinated regulatory strategy for lignocellulose degradation in filamentous fungi. In plant cell walls, cellulose is closely associated with hemicellulose, and early cellulose hydrolysis can generate soluble oligosaccharides that function as signaling molecules to trigger broader lignocellulolytic responses. These signals are integrated through global transcriptional regulators such as XlnR/Xyr1, which coregulate both cellulase and xylanase gene expressions, thereby ensuring synergistic degradation of complex biomass substrates.[44,45] Beyond transcriptional coregulation, such a response may be advantageous for white-rot fungi, as cellulose and hemicellulose are tightly associated within plant cell walls and are typically degraded through the coordinated action of cellulolytic and hemicellulolytic enzyme systems. Therefore, the stronger induction of PeXyn1 by cellulose may reflect an adaptive strategy that promotes the simultaneous activation of lignocellulose-degrading enzymes, thereby facilitating the efficient utilization of complex plant biomass.[46] The time-

https://doi.org/10.1021/acs.jafc.6c05044
J. Agric. Food Chem. XXXX, XXX, XXX−XXX

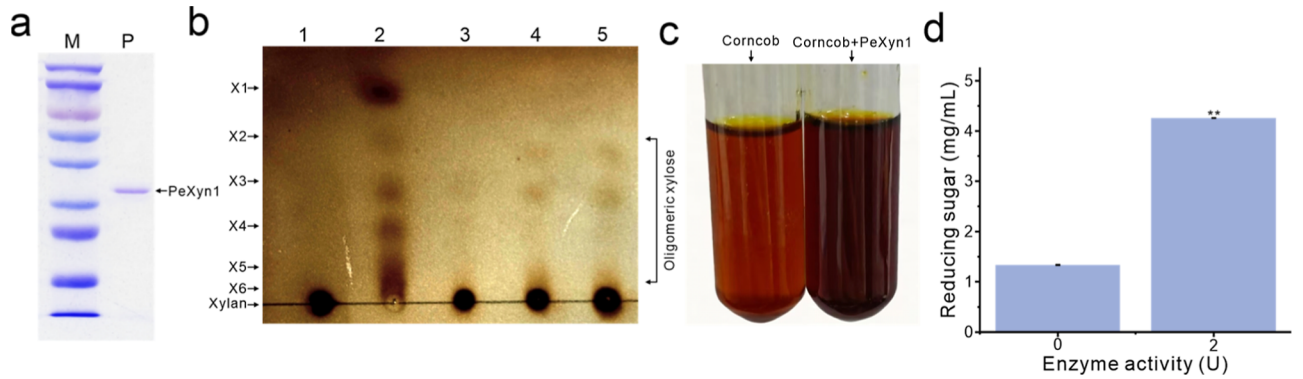

Figure 3. Purification and catalytic characterization of the recombinant PeXyn1. (a) SDS-PAGE analysis of partially purified PeXyn1. Line M, standard marker proteins; lane P, recombinant PeXyn1. (b) TLC analysis of beechwood xylan hydrolysis by PeXyn1. Lane 1, beechwood xylan substrate; lane 2, xylo-oligosaccharide standards (X1−X6); lanes 3−5, hydrolysis products obtained after incubation with PeXyn1 for 0.5, 1, and 2 h, respectively. (c) Colorimetric detection of reducing sugars released by PeXyn1 versus the untreated control (CK). (d) Quantitative analysis of the reducing sugar yield produced by PeXyn1 relative to the CK.

course induction of xylanase activities by cellulose in *P. eryngii* was measured from 0 to 48 h. The results showed a significant increase in xylanase activity starting at 24 h of induction, which continued to rise and peaked at 7.52 ± 0.23 U mL^{-1} at 48 h (Figure 1a). This trend in enzyme activity was consistent with that observed for cellulase (Figure 1b).

To identify key extracellular xylanases induced by cellulose, an integrated comparative proteomic and transcriptomic analysis was performed. Proteomic profiling of the culture secretome identified six xylanases, including two GH11 family members and four GH10 family members. Among these, three xylanases (KAF9492119, KAF9492116, and KAF9501169) exhibited significantly increased abundance in cellulose-induced samples, while the other three xylanases were uniquely detected under induction conditions (Table 1). Parallel transcriptomic analysis further validated these findings, revealing that five xylanase genes were significantly upregulated (more than 10-fold) at the transcriptional level at 36 h (Table 1). These multiomics results collectively confirmed that cellulose could induce the expression of xylanases in *P. eryngii* at both the transcriptional and translational levels. On the basis of their expression profiles, the two highly expressed GH11 candidates (KAF9492119 and KAF9492116) were selected for cloning. One target gene was successfully cloned and designated as PeXyn1. In agreement with the omics results, RT-qPCR analysis revealed that the transcription level of *PeXyn1* remained relatively stable during the initial 24 h but increased sharply after 36 h, reaching a peak of a 26.87-fold increase at 48 h (Figure 1c). The nucleotide sequence of *PeXyn1* has been deposited in the GenBank database under accession number PZ136043.

3.2. Phylogenetic Analysis and Structural Architecture of PeXyn1

The amino acid sequence of PeXyn1 showed 99.21% and 87.01% sequence identity with KAF9492116 and KAF9492119, respectively. These sequence variations may be attributed to strain-specific differences within *P. eryngii*. Furthermore, PeXyn1 shares only 75.63% amino acid sequence identity with its closest functionally characterized homologue, endo-1,4-β-xylanase A from *Schizophyllum commune* (P35809).

Endo-β-1,4-xylanases are predominantly categorized into the GH11 family; however, a significant proportion also belongs to the GH10, GH5, GH8, GH30, and GH43 families. To elucidate its evolutionary position, a phylogenetic tree was constructed using PeXyn1, KAF9492116, KAF9492119, and 19 other functionally characterized xylanases from GH11 (Figure 2a). Beyond KAF9492116 and KAF9492119, PeXyn1 exhibits the closest evolutionary proximity to P35809 from *S. commune*. Interestingly, despite their common basidiomycetous origin, PeXyn1 is evolutionarily distant from the xylanase of *Lentinula edodes* (AAL04152) and that of *Phanerochaete chrysosporium* (B7SIW1), which cluster in a separate major clade. As shown in Figure 2a, the topological structure of the tree does not strictly mirror fungal species phylogeny. This discrepancy might be driven by extensive early gene duplication and expansion within the fungal GH11 family, which has led to high sequence diversity facilitating adaptation to complex lignocellulosic substrates.[47] Besides, since the genomes of most basidiomycetous edible fungi harbor multiple xylanases, only a fraction of these have been cloned and characterized to date. Consequently, the distinct clades presented in the tree likely represent paralogous genes (paralogs) with divergent evolutionary histories, which may have evolved differences in substrate specificity, catalytic modes, or environmental adaptability.[48,49]

Sequence analysis (Figure 2a) identified several conserved motifs in PeXyn1 that align precisely with the canonical architecture of basidiomycetous GH11 enzymes. PeXyn1's catalytic competency is governed by two highly conserved glutamate residues (Glu^{103} and Glu^{200}) positioned within the classic β-jelly roll fold of the GH11 active site (Figure 2b), consistent with the canonical double-displacement mechanism. Multiple sequence alignment (Figure 2c) revealed highly conserved motifs flanking the catalytic nucleophile, conforming to the consensus patterns PL[IV]EYY[IV]V[ED][SN][YF] and [IV][VL][AS][TV]E[GA][YW][QFS][SG][SA]G[ST]-[AS]. Sequence analysis confirms the conservation of these residues and their flanking sequences, including proximal tyrosine residues that likely assist in substrate recognition via aromatic stacking.[50,51]

Furthermore, PeXyn1 is characterized by a multidomain architecture comprising the GH11 catalytic core and a C-terminal carbohydrate-binding module (CBM1) domain. Connecting these domains is a serine-rich linker (residues 223−255: SSGSSTISVSEGGSSGGGSPTSSTPPAQSSTPS) (Supporting Information, Figure S2), which likely maintains structural integrity and flexibility, analogous to the linker

https://doi.org/10.1021/acs.jafc.6c05044
J. Agric. Food Chem. XXXX, XXX, XXX−XXX

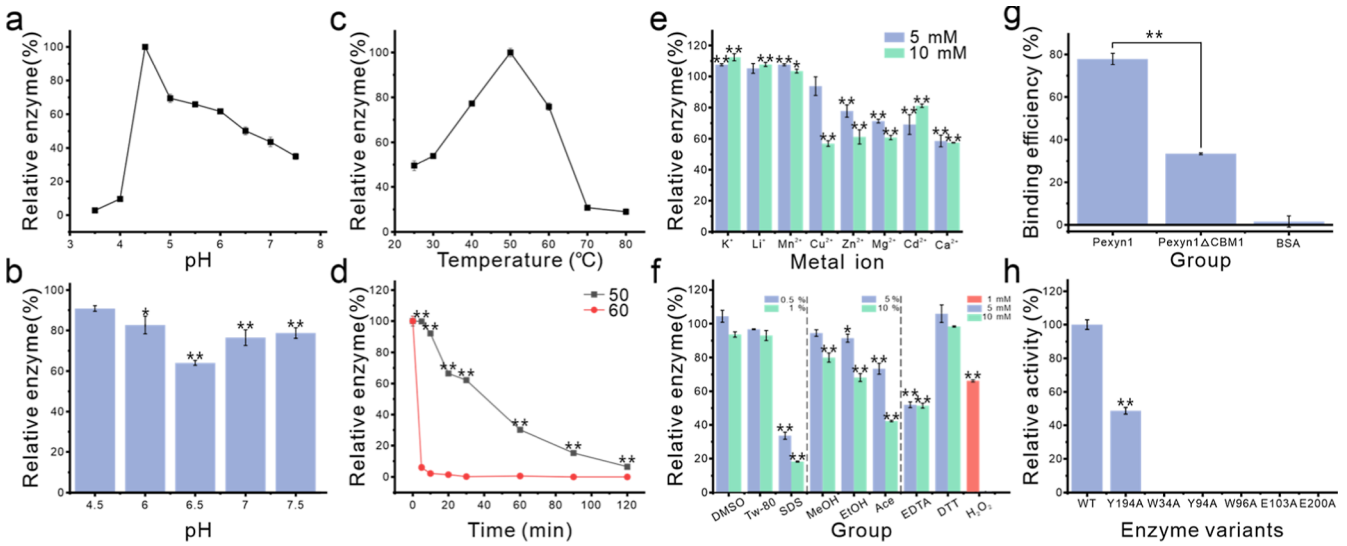

Figure 4. Enzymatic properties of purified recombinant PeXyn1. (a) Optimum pH of xylanase activity. (b) pH stability profile, showing the residual activity after preincubation of the enzyme at different pH levels. (c) Optimal temperature for xylanase activity, measured across a temperature range of 25−80 °C. (d) Thermostability of PeXyn1, depicting the residual enzyme activity after incubation at 50 and 60 °C for various time intervals up to 120 min. Influence of different metal ions (e) and chemical compounds (f) on PeXyn1 activity. (g) Binding efficiency (%) of PeXyn1, PeXyn1ΔCBM1, and BSA to substrate. (h) Relative activities (%) of WT and selected xylanase mutants.

function in other multidomain glycoside hydrolases.[52] This CBM1 domain is critical for function; its aromatic residues (Trp^{263}, Trp^{271}, Tyr^{281}, Tyr^{289}, and Tyr^{290}) serve as putative binding sites that anchor the enzyme and disrupt crystalline substrate structures, while also contributing to thermal stability.[53,54] Although removing the CBM1 might enhance specific activity on soluble xylan, its presence is essential for the efficient saccharification of complex substrates like bagasse.[55−57] This necessity arises because, in natural lignocellulosic biomass, xylan tightly coats and cross-links with cellulose microfibrils. By possessing a cellulose-binding CBM1 domain, PeXyn1 can anchor firmly to the exposed cellulose scaffold, creating a "proximity effect" that keeps the GH11 catalytic core in close contact with its target xylan network.[58]

To further resolve the functional and evolutionary patterns of CBM1-containing modular xylanases in *P. eryngii*, we investigated the distribution of these domains across our proteomic profiles and other published data sets under varying cultivation conditions (Table S3). Under conditions with simple or soluble carbon sources, the number of expressed xylanases was minimal and those harboring a CBM1 domain were completely absent.[33] In contrast, when *P. eryngii* was challenged with recalcitrant, insoluble lignocellulosic substrates such as cellulose powder or wheat straw, the total number of secreted xylanases increased significantly, accompanied by the specific recruitment of CBM1-containing variants from both the GH10 and GH11 families.

3.3. Heterologous Expression and Catalytic Properties of PeXyn1

Pichia pastoris is a suitable host for eukaryotic protein expression.[59,60] Therefore, the *PeXyn1* gene was expressed in *P. pastoris* GS115. Following ammonium sulfate precipitation and nickel affinity purification, PeXyn1 was purified as a single band in SDS-PAGE (Figure 3a). The apparent MW was close to, but slightly higher than, the theoretical value and was lower than that reported for xylanases from *L. edodes*.[61] The optimal xylanase expression condition was at 28 °C in a buffer-free system instead of the PBS buffer (Supporting Information, Figure S3a,b). This phenomenon is likely attributed to the natural acidification of the unbuffered medium, which inhibits endogenous neutral/alkaline proteases and thereby reduces proteolytic degradation of the recombinant protein.[62] Furthermore, supplementation with Zn^{2+} significantly enhanced enzymatic activity by day 9 (Supporting Information, Figure S3c). This enhancement is attributed to zinc's role as an essential cofactor for zinc-finger transcription factors that upregulate methanol metabolism genes,[63] a mechanism substantiated by the observed low methanol consumption (Supporting Information, Figure S3d).

Purified PeXyn1 could hydrolyze xylan to reducing sugars as detected by the DNS assay method. According to TLC analysis (Supporting Information, Text S8), the hydrolysis of xylan by PeXyn1 yielded a diverse array of xylo-oligosaccharides in a time-dependent manner (Figure 3b). The progressive accumulation of these oligosaccharides clearly indicates that PeXyn1 functions primarily as an endoxylanase, consistent with the in silico analysis above. The hydrolytic capacity of the purified enzyme on a raw agricultural substrate was evaluated using corncob (120 mesh) as the substrate (Supporting Information, Text S9). As visually demonstrated by the DNS assay (Figure 3c), the PeXyn1-treated reaction mixture exhibited a deep reddish-brown color indicative of high reducing sugar concentrations. The application of PeXyn1 led to a substantial release of reducing sugars, showing a remarkable fold increase over the control and achieving a maximum yield of 4.258 ± 0.001 mg mL^{-1} (Figure 3d) at 2 h. This underscores the immense potential of PeXyn1 as a robust biocatalyst for industrial lignocellulose bioconversion and agro-waste valorization.[64]

PeXyn1 exhibits an acidic pH optimum of 4.5 (Figure 4a) and demonstrates remarkable stability across a broad range (pH 4.5−7.5), retaining >60% activity after 24 h (Figure 4b). This alkali tolerance, similar to recombinant *L. edodes* xylanase,[65] suggests utility in processes requiring pH fluctuation.[32] Thermally, PeXyn1 functions as a mesophilic enzyme with an optimal temperature of 50 °C (Figure 4c).

https://doi.org/10.1021/acs.jafc.6c05044
J. Agric. Food Chem. XXXX, XXX, XXX−XXX

While lacking the hyper-thermostability of *Thermomyces lanuginosus* or *Thermotoga naphthophila* enzymes,[66−68] its thermal profile resembles that of *Aspergillus oryzae* and *Penicillium citrinum* xylanases,[69−71] retaining >50% activity after 40 min at 50 °C (Figure 4d). K^+ and Mn^{2+} significantly promoted enzymatic activity (Figure 4e). The activation by Mn^{2+} aligns with previous reports[72] and may involve the stabilization of the active site conformation. In contrast, Cu^{2+} exerted strong inhibition (reducing activity to 56.76 ± 1.79% at 10 mM), a common trait among xylanases,[73,74] potentially caused by Cu^{2+}-induced hydrophobic shifts in tryptophan/tyrosine microenvironments or disulfide bond disruption.[75] Additionally, the enzyme tolerated organic solvents like acetone (>40% residual activity) but was sensitive to SDS and H_2O_2; the latter caused near-total activity loss, likely due to the oxidation of critical tryptophan/methionine residues,[76] while activity enhancement by 5 mM DTT suggests that preventing cysteine oxidation benefits catalytic performance (Figure 4f). White-rot fungi utilize H_2O_2 as an essential cosubstrate for lignin-degrading oxidoreductases to breach the lignin barrier.[77] The severe oxidative inactivation of PeXyn1 suggests that hemicellulose hydrolysis should be separated from this oxidative burst. This evolutionary adaptation likely ensures that hydrolytic enzymes like PeXyn1 function optimally only in protective microenvironments or at later decay stages, after the H_2O_2-driven ligninolysis has concluded, thereby safely coordinating the complete depolymerization of biomass.[78,79]

Purified PeXyn1 exhibited strict substrate specificity for xylan, with the highest affinity for beechwood xylan followed by corncob xylan (Table 2), with no activity on CMC-Na or starch. While previous studies have shown that xylanase production in *P. eryngii* can be induced by starch,[80] a feature similar to that observed in our study, purified PeXyn1 strictly lacks any cellulolytic background activity. This aligns perfectly with specialized purified GH11 xylanases from other edible mushrooms, such as *L. edodes* (Xyn11A)[65] and *Termitomyces clypeatus*,[81] which also demonstrate no cellulase activity. Kinetic analysis under optimal conditions yielded a K_m of 27.51 mg mL^{-1} for beechwood xylan, with a corresponding turnover number k_{cat} of 20.95 s^{-1} and a catalytic efficiency k_{cat}/K_m of 0.76 $mL \cdot mg^{-1} \cdot s^{-1}$ (Table 3). Previous characterizations of GH11 fungal xylanases using beechwood xylan have revealed a broad spectrum of K_m values, ranging from highly sensitive enzymes like that of *Penicillium oxalicum* GZ-2 (3.0 mg mL^{-1})[82] to those with moderate affinities, such as *Aspergillus tamarii* (8.13 mg mL^{-1})[83] and *Trichoderma* sp. (19.12 mg mL^{-1}).[84] To specifically contextualize its catalytic efficiency among edible mushrooms, the kinetic parameters of PeXyn1 were further compared with previously reported xylanases from these species. For instance, a recombinant xylanase (Xyn11A) cloned from *L. edodes* exhibited a K_m of 1.5 mg mL^{-1} for birchwood xylan.[65] Similarly, an inducible purified xylanase from *T. clypeatus* showed a K_m of 4 mg mL^{-1}.[81] Furthermore, kinetic studies utilizing crude xylanase extracts from *P. eryngii* MTCC 1798 reported a K_m of 7.21 mg mL^{-1}.[80] Compared to these highly sensitive enzymes, the elevated K_m of PeXyn1 indicates a high saturation threshold. This elevated K_m value suggests that PeXyn1 remains catalytically active across a broad range of substrate concentrations.[85] Such a characteristic may reduce premature enzyme saturation under substrate-rich conditions,[86] thereby supporting sustained catalytic rates and potentially facilitating the efficient processing of lignocellulosic materials at high substrate loadings. The industrial relevance of PeXyn1 is underscored by its robust operational stability in acidic environments, presenting a distinct advantage over the highly variable pH optima reported for *P. eryngii* crude extracts. Structurally, PeXyn1 features a modular architecture comprising a GH11 catalytic core and a C-terminal CBM1 domain, analogous to the architecture of *L. edodes* Xyn11A.[65] This modular architecture circumvents the limitations of single-domain GH11 xylanases, facilitating dynamic interactions with complex agro-industrial waste matrices. While previous studies have extensively investigated crude xylanolytic activities from *P. eryngii*, to the best of our knowledge, PeXyn1 represents the first specific xylanase gene to be heterologously expressed and functionally characterized from this species.

Table 2. Substrate Specificity of Xylanase PeXyn1

substrates	concentration (%)	relative activity (%)
beechwood xylan	0.4	100
corncob xylan	0.4	21.12 ± 1.69
starch	0.4	0.84 ± 0.25
β-cyclodextrin	0.4	0
CMC	0.4	0

Table 3. Steady-State Kinetic Parameters of PeXyn1 and Its Variants

variants	K_m (mg mL^{-1})	V_{max} (mol min^{-1} mg^{-1})	k_{cat} (s^{-1})	k_{cat}/K_m (mL mg^{-1} s^{-1})
PeXyn1△CBM1	30.56	1.51×10^{-4}	61.93	2.03
PeXyn1	27.51	4.41×10^{-5}	20.95	0.76
PeXyn1-Y194A	14.19	1.55×10^{-5}	7.33	0.52

3.4. Impact of the CBM1 Domain on PeXyn1 Enzymatic Activity and Kinetics

While *P. pastoris* is ideal for studying eukaryotic modifications, high-level and cost-effective expression in *E. coli* is essential for industrial production.[87] The xylanase was heterologously expressed in *E. coli*, and the recombinant enzyme retained its catalytic activity. Since *E. coli* lacks the eukaryotic post-translational glycosylation machinery, this functional expression indicates that either the native xylanase is not glycosylated or that glycosylation is not essential for its hydrolytic activity. Singh et al.[88] also successfully expressed an active xylanase from the fungus *Chaetomium globosum* in *E. coli*, which is highly consistent with our findings. Furthermore, to investigate whether the carbohydrate-binding module (CBM1) of PeXyn1 plays a critical role in catalysis, we constructed a CBM1-truncated variant and heterologously expressed it in *E. coli* cells. Both the mature PeXyn1 and the truncated PeXyn1ΔCBM1 were successfully expressed using the pET-28a vector. SDS-PAGE confirmed their soluble expression (Supporting Information, Figure S4). To investigate the role of the CBM1 domain, their specific activities and kinetics on beechwood xylan were compared. The specific activity of the full-length enzyme increased significantly from 10.04 ± 0.29 U mg^{-1} to 28.79 ± 2.23 U mg^{-1} upon CBM1 truncation. Consistent with this, PeXyn1ΔCBM1 showed a slightly increased K_m (30.56 mg mL^{-1}) (Table 3). These results demonstrate that CBM truncation does not impair soluble xylan hydrolysis; instead, it improves overall specific activity

https://doi.org/10.1021/acs.jafc.6c05044
J. Agric. Food Chem. XXXX, XXX, XXX−XXX

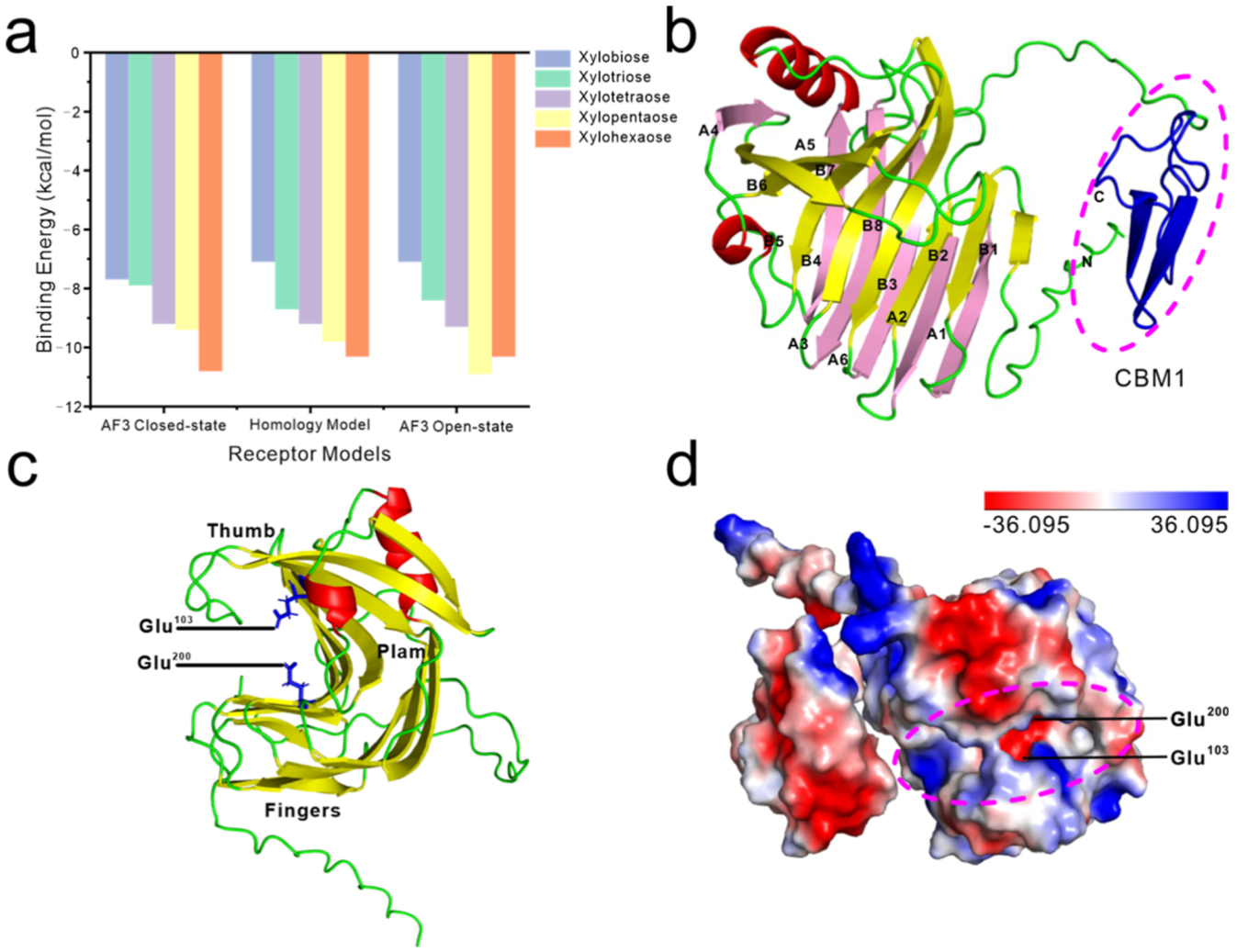

Figure 5. Three-dimensional structure and electrostatic surface potential of PeXyn1. (a) Binding energies of different PeXyn1△CBM1 structural models (AlphaFold 3 open/closed states, and a homology model based on template A0A067NH24) with various xylooligosaccharides. (b) Overall ribbon representation of PeXyn1, illustrating two β-sheets packed against each other and flanked by α-helices. (c) The canonical "right-hand" conformation characteristic of GH11 xylanases, comprising the Thumb, Palm, and Finger regions. The catalytic residues (Glu^{103} and Glu^{200}) are highlighted as blue sticks. (d) Electrostatic potential surface map of PeXyn1.

and catalytic turnover, likely by reducing steric hindrance. This confirms that the GH11 catalytic core is highly competent for soluble substrate depolymerization,[89] whereas the CBM is primarily required for targeting and anchoring the enzyme to complex, insoluble lignocellulosic matrices.[90] To directly validate this anchoring function, an in vitro binding assay using Avicel was performed (Figure 4g; Supporting Information, Text S10), and the corresponding activity changes were further assessed (Figure 4h). The full-length PeXyn1 exhibited a high binding efficiency of approximately 78%. In contrast, the truncated PeXyn1ΔCBM1 showed a significantly reduced binding capacity (~33%), while the negative control (BSA) displayed negligible binding. These empirical results substantiate that the CBM1 domain is essential for physically tethering the enzyme to insoluble substrates, providing robust evidence for the proposed proximity effect.

3.5. The Binding Mechanism of Xylan and Xylanase

To determine the optimal initial conformation for subsequent simulations, molecular docking of xylo-oligosaccharides was performed on the catalytic domain (excluding the CBM1 domain) using three receptor models: the AF3 open-state, the AF3 closed-state, and a SWISS-MODEL homology model (Figure 5a). Because the binding energies showed only minor differences among the models, the AF3 open-state structure was selected for further analysis. Its more accessible active cleft better accommodates initial substrate entry and facilitates the observation of the dynamic induced-fit closure mechanism during molecular dynamics simulations. The protein structure predicted by AlphaFold3 reveals that the tertiary structure of PeXyn1 adopts the canonical GH11 β-jelly roll topology, comprising two α-helices and 14 antiparallel β-strands (Figure 5b). This forms a "right-handed" conformation where the loop connecting strands B6 and B7 constitutes a specific "Thumb" structure (Figure 5c and Supporting Information, Figure S5). Consistent with the crystal structures of GH11 enzymes, this region partially encloses the active cleft while imparting flexibility.[91] The curved β-sheet B8 and the "Thumb" define a deep active cleft capable of accommodating approximately six xylose units, aligning with classical descriptions of the GH11 active center.[92] Electrostatic potential analysis (Figure 5d) indicates a range from −36.095 to 36.095 kT/e. Despite an uneven overall surface charge, the electronegative environment

https://doi.org/10.1021/acs.jafc.6c05044
J. Agric. Food Chem. XXXX, XXX, XXX−XXX

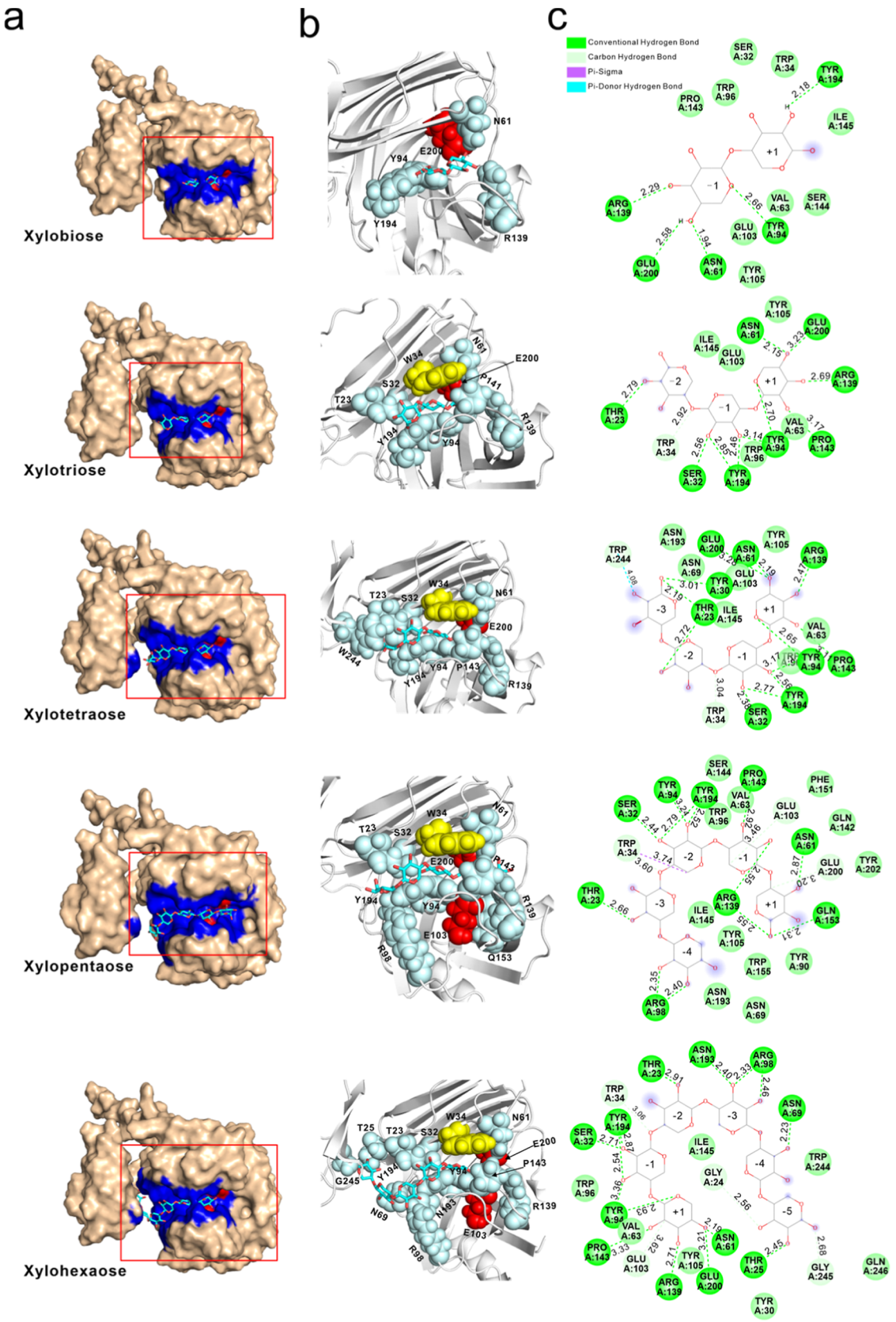

Figure 6. Molecular docking models of PeXyn1 with xylooligosaccharides (XOSs). (a) Surface views of PeXyn1 docked with xylobiose through xylohexaose. Residues located within 6 Å of the substrates are highlighted in blue, while the two catalytic residues are shown in red. (b) Detailed close-up views of the active site. Substrates are shown as cyan sticks. Key residues are shown as spheres: cyan for direct interaction, yellow for proximity to glycosidic bonds, and red for catalytic glutamates (Glu^{103} and Glu^{200}). (c) 2D schematic diagrams (LigPlot) of protein–ligand interactions. Hydrogen bonds are indicated by dashed lines, and numbers represent distances between residues and ligands in Angstroms (Å).

https://doi.org/10.1021/acs.jafc.6c05044
J. Agric. Food Chem. XXXX, XXX, XXX−XXX

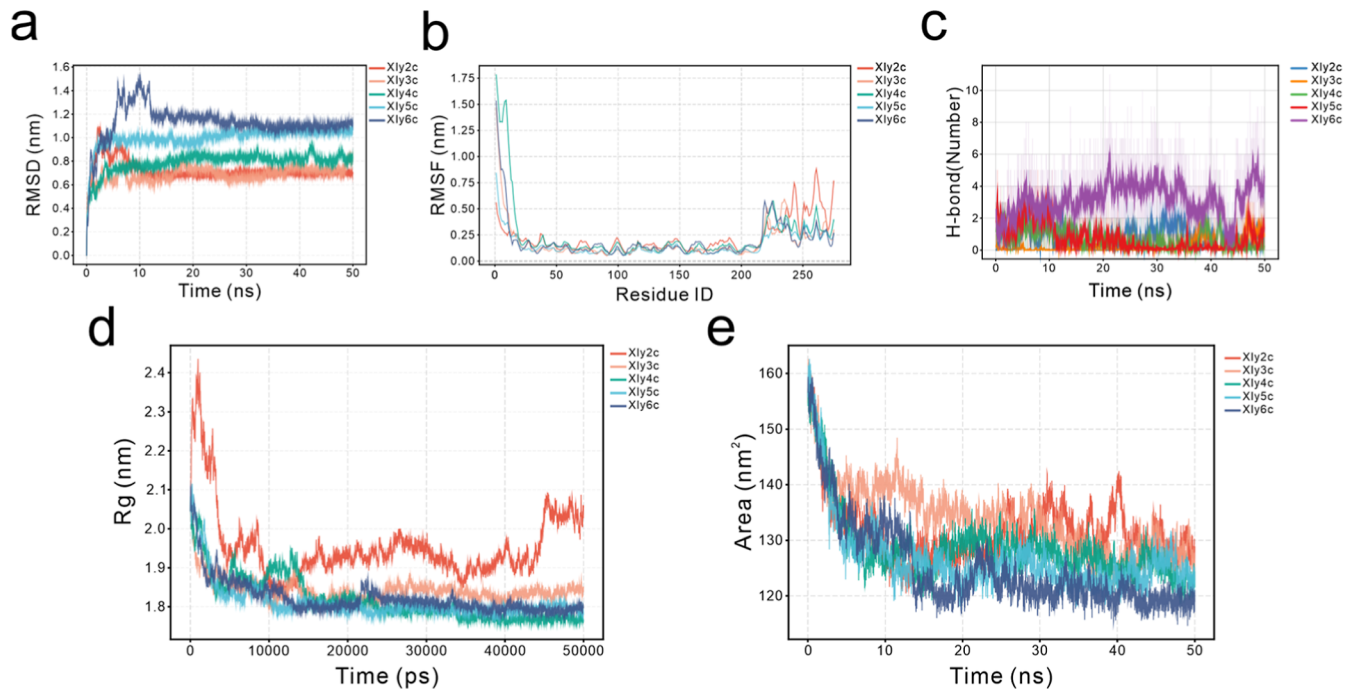

Figure 7. Molecular dynamics (MD) simulation analysis of PeXyn1 complexed with different xylooligosaccharides (X2-X6) over 50 ns. (a) Root-mean-square deviation (RMSD) values of the backbone atoms. (b) Root-mean-square fluctuation (RMSF) of the amino acid residues. (c) Number of intermolecular hydrogen bonds between PeXyn1 and the respective substrates. (d) Radius of gyration (R_g) of the complexes. (e) Solvent-accessible surface area (SASA) of the complexes during the simulation.

of the active center remains consistent regardless of substrate chain length in molecular docking results using AutoDock Vina (Supporting Information, Figure S6). Furthermore, docking simulations show that the substrate contact surface area increases significantly upon binding longer substrates (Supporting Information, Table S4), strongly suggesting a potential induced-fit mechanism.

Molecular docking elucidated the binding details of PeXyn1 with xylans of varying degrees of polymerization (Figure 6). The active pocket forms a long, deep cleft (Figure 6a) lined with aromatic and polar residues (Arg^{139} and Asn^{61}). Notably, Trp^{34} and Tyr^{94} act as a "clamp" flanking the sugar ring (Figure 6b), theoretically providing steric hindrance to limit substrate sliding while creating a stabilizing hydrophobic environment.[93] Substrate recognition heavily relies on aromatic stacking within a hydrophobic platform formed by Tyr^{194}, Tyr^{94}, Trp^{96}, Trp^{34}, Tyr^{105}, and Trp^{244}. Specifically, Trp^{34} forms weak hydrogen bonds and pi−sigma interactions, theoretically contributing to active center rigidity and thermal stability.[94] Within this cleft, conserved catalytic residues Glu^{103} and Glu^{200} flank the glycosidic bond to catalyze hydrolysis (Figure 6b).[95] Complex stability is primarily driven by hydrogen bonding, increasing from 5 bonds in xylobiose to 15 in xylohexaose (Figure 6c). While Tyr^{194} and Tyr^{94} anchor the O_2 and O_3 atoms, Glu^{200} bonds primarily with short-chain substrates. For pentamers and longer chains, both Glu^{103} and Glu^{200} interact with substrate carbon atoms. To robustly validate these docking interactions, site-directed mutagenesis was performed on these predicted key residues (Figure 4h; primers listed in Supporting Information, Table S2). The substitution of the catalytic residues (E103A and E200A) resulted in a complete loss of enzymatic activity, confirming their indispensable role in hydrolysis.[94] Furthermore, alanine mutations of the crucial aromatic residues forming the hydrophobic platform and the proposed substrate "clamp" (W34A, Y94A, and W96A) also completely abolished activity. This profound loss of function directly substantiates our structural observation that Trp^{34} and Tyr^{94} constitute an essential clamp mechanism strictly required for securing the substrate. The Y194A mutation retained approximately 48% of the wild-type activity and showed markedly impaired kinetic performance (Table 3). While the decreased K_m value indicates stronger substrate binding, the reduced catalytic activity suggests that Tyr^{194} plays a critical role in facilitating productive substrate orientation and transition-state stabilization, thereby supporting efficient catalysis rather than being strictly required for substrate recognition. Bond length analysis reveals interaction range from 1.94−2.66 Å for xylobiose, extending up to 3.36 Å for longer substrates due to increased conformational freedom of the extended chains (Figure 6c). Binding energy calculations revealed a strong chain-length dependency for full-length PeXyn1, with affinity peaking for xylohexaose (−11.7 kJ mol^{-1}) and weakening to −7.2 kJ mol^{-1} for xylobiose (Supporting Information, Table S4). This indicates that the affinity increases significantly with chain length,[96] demonstrating the potential high adaptability of PeXyn1 for long-chain xylo-oligosaccharides.

To evaluate potential steric interference by the CBM1, a truncated model was docked with xylopentaose and xylohexaose using AutoDock Vina (Supporting Information, Figure S7; Table S5). The binding posture remained highly consistent with the full-length protein, indicating no significant steric hindrance from the CBM1 (Supporting Information, Figure S7a). The catalytic pair Glu^{103} and Glu^{200} maintained precise anchoring (Supporting Information, Figure S7b). However, without CBM1, the Glu^{103}-xylopentaose interaction shifted from C5 to C3 (Supporting Information, Figure S7c). Interactions involving CBM1 residues (Trp^{244}, Gly^{245}, and

https://doi.org/10.1021/acs.jafc.6c05044
J. Agric. Food Chem. XXXX, XXX, XXX−XXX

Gln^{246}) disappeared, while Tyr^{202} stabilization at the substrate terminus became prominent, making aromatic stacking effects more pronounced.[97] Molecular modeling performed with AlphaFold3 further suggests a possible interaction between the CBM1 domain and the substrate (Supporting Information, Figure S8). Docking results revealed that high-polymerization substrates were predicted to additionally engage Asn^{88} via hydrogen bonding. The catalytic core maintains electrostatic independence without the CBM1, meaning that the CBM1 domain assists in anchoring without altering the physicochemical microenvironment (Supporting Information, Figure S6). Notably, the truncation of the CBM1 domain reduced the binding affinity for xylohexaose to −10.3 kJ mol^{-1}, while the affinity for xylobiose remained largely unchanged (−7.1 kJ mol^{-1}) (Supporting Information, Table S6). Ultimately, the stronger affinity energy in the mature protein suggests that the CBM1 domain may contribute to stabilizing the substrate binding conformation. Therefore, the proposed contribution of CBM1 to the stabilization of longer xylo-oligosaccharides should be regarded as a structural prediction that requires further experimental validation. Crucially, our in vitro binding assay (Figure 4g) empirically demonstrated the indispensable role of the CBM1 domain in physically anchoring PeXyn1 to the insoluble substrates.

Interestingly, while the removal of the CBM1 domain may enhance the specific activity of the enzyme against soluble substrates under in vitro experimental conditions, both our structural analysis and existing literature underscore its vital role in binding long-chain substrates.[93] In the highly complex and insoluble lignocellulosic matrix of natural environments, this enhanced affinity for longer chains provided by the CBM1 is likely indispensable.[90] By efficiently anchoring the enzyme to the extended polysaccharide networks, the CBM1 domain facilitates sustained, localized hydrolysis,[98] thereby potentially conferring a critical ecological advantage for the efficient degradation of solid biomass by *P. eryngii*.

3.6. Molecular Dynamics Simulations of PeXyn1 with DP 2−6 Xylo-Oligosaccharides

To evaluate the structural stability of PeXyn1 upon binding to xylo-oligosaccharides of varying polymerization degrees, molecular dynamics (MD) simulations were performed. In the initial phase (0−10 ns), the root-mean-square deviation (RMSD) values of all systems increased sharply before converging to a stable fluctuation range, indicating a sufficient simulation duration to reach equilibrium.[96] During equilibrium, the average backbone RMSD displayed a gradual upward trend correlated with the substrate length. Complexes with short-chain substrates stabilized at lower RMSD levels. Conversely, longer xylan chains slightly increased steady-state RMSD values and fluctuation amplitudes. This suggests substrate-induced conformational adjustments rather than structural destabilization, as all systems remained well equilibrated throughout the simulation (Figure 7a). This interpretation is further supported by the ligand RMSD analysis. In contrast to the protein backbone (Supporting Information, Figure S9a), the ligand RMSD exhibited an inverse trend (Supporting Information, Figure S9b). Short-chain substrates showed high fluctuations, whereas long-chain ligand RMSD curves became significantly flatter with lower mean values. Notably, the X6 system ligand maintained a low fluctuation amplitude, indicating stable anchoring within the catalytic center.[96] Root-mean-square fluctuation (RMSF) analysis (Figure 7b) revealed high rigidity in the catalytic domain (residues 18−216) across all systems. The CBM1 domain (residues 239−275) exhibited higher fluctuations, but its amplitude was negatively correlated with substrate length. Reduced flexibility in the C-terminal region has been associated with improved thermostability,[99] indicating that long-chain substrates effectively restrict CBM1 motions and contribute to regional stabilization.

During the simulations, hydrogen bonds formed between PeXyn1 and xylo-oligosaccharides (Figure 7c), peaking in the X6 system with an average of 10−12 bonds. This robust hydrogen-bond network provides a structural basis for the reduced CBM1 flexibility observed in the RMSF analysis. Extended glycan chains occupied the −2 to +1 subsites and reached distal subsites, forming direct hydrogen bonds with the CBM1. This enhanced hydrogen bonding is inferred to strengthen structural rigidity and lock the enzyme's conformation, which may improve thermodynamic stability.[100,101] With increasing substrate length, the complex's radius of gyration (R_g) and total solvent-accessible surface area (SASA) gradually decreased (Figure 7d, e), stabilizing near 1.8 and 120 nm^2, respectively. A low R_g state combined with extensive hydrogen bonding suggests that the catalytic and CBM1 domains are drawn tightly together. Since substrate binding is accompanied by desolvation, the reduced SASA suggests effective shielding of hydrophobic regions within the active-site cleft and binding channel, consistent with decreased solvent accessibility and enhanced stabilization of the enzyme−substrate complex.[96,102] Collectively, the MD analyses support a substrate-induced stabilization model. Although longer xylo-oligosaccharides caused modest increases in backbone RMSD, indicative of conformational adaptation, they simultaneously reduced ligand mobility and CBM1 flexibility, promoted the formation of a more extensive hydrogen-bond network, and decreased both R_g and SASA values. Together, these coordinated changes support a transition toward a more compact and conformationally restrained state, in which long-chain substrates stabilize the enzyme through multivalent interactions with the bound ligand, potentially facilitating substrate recognition and catalysis.

Overall, this study identified and characterized PeXyn1, a cellulose-upregulated GH11 xylanase from *P. eryngii*, containing a C-terminal CBM1 domain. Recombinant PeXyn1 exhibited broad pH stability, Mn^{2+}-dependent activation, and high specificity for xylan-rich agricultural biomass. Combined structural, biochemical, and molecular dynamics analyses revealed that long-chain substrates promote a compact and thermodynamically stable enzyme conformation through extensive hydrogen-bonding interactions between the catalytic core and the CBM1 domain. These findings provide mechanistic insights into CBM1-mediated substrate recognition and offer a foundation for the engineering of fungal xylanases for an efficient lignocellulosic biomass conversion.

■ ASSOCIATED CONTENT

Data Availability Statement

This article does not contain any studies with human participants or animals performed by any of the authors.

Supporting Information

The Supporting Information is available free of charge at https://pubs.acs.org/doi/10.1021/acs.jafc.6c05044.

https://doi.org/10.1021/acs.jafc.6c05044
J. Agric. Food Chem. XXXX, XXX, XXX−XXX

3D protein structures, molecular docking complexes, and MD simulation models of PeXyn1 and PeXyn1ΔCBM1 with xylo-oligosaccharides (ZIP)

Culture media and formulations used in this study, protein extraction and bioinformatics analysis of *P. eryngii* mycelia, extracted total RNA, RNA sequencing and bioinformatics analysis, amplification and cloning of *PeXyn1* gene. recombinant strains expression, expression in *E. coli*, analysis of hydrolysis products, enzymatic hydrolysis of lignocellulosic substrates by PeXyn1, substrate binding assay, time-course of cellulase and xylanase activity induction in *P. eryngii* by cellulose and xylan, multiple sequence alignment of the sequence of xylanase PeXyn1 and related basidiomycete xylanases, optimization of induction conditions for recombinant GS115 xylanase expression, SDS-PAGE analysis of recombinant PeXyn1 forms expressed in *E. coli*, amino acid sequence and predicted secondary structure of xylanase PeXyn1, surface electrostatic potential of the mature protein and catalytic domain in complex with xylo-oligosaccharides, molecular docking analysis of the truncated PeXyn1 (catalytic domain only) with xylo-oligosaccharides, molecular docking models of xylanase PeXyn1 with xylo-oligosaccharides, time-dependent root-mean-square deviation (RMSD) profiles during the 50 ns MD simulations, optimization of enzymatic hydrolysis conditions for the recombinant xylanase, sequence of RT−qPCR primers used in this study, sequence and function of primers used in this study, distribution patterns of CBM1-containing xylanases in various *P. eryngii* secretomes, binding affinities and pocket volumes of the optimal docking complexes of PeXyn1, binding affinities of the optimal docking complexes of PeXyn1△CBM1, and physicochemical properties of xylanases used in evolutionary analysis (PDF)

AUTHOR INFORMATION

Corresponding Authors

Hailong Yu − *National Engineering Research Center of Edible Fungi, Institute of Edible Fungi, Shanghai Academy of Agricultural Sciences, Shanghai 201403, China*; Email: yuhailong@saas.sh.cn

Hao Yu − *Shandong Provincial Key Laboratory of Applied Mycology, School of Life Sciences, Qingdao Agricultural University, Qingdao 266109, China*; orcid.org/0000-0002-1892-7993; Email: yuhaosunshine@163.com

Authors

Xiaohang Li − *Shandong Provincial Key Laboratory of Applied Mycology, School of Life Sciences, Qingdao Agricultural University, Qingdao 266109, China; Key Laboratory of Marine Environment and Ecology, College of Environmental Science and Engineering, Ocean University of China, Qingdao 266100, China*

Xianfeng Du − *Shandong Provincial Key Laboratory of Applied Mycology, School of Life Sciences, Qingdao Agricultural University, Qingdao 266109, China*

Yan Zhang − *Shandong Agricultural Technology Extending Station, Jinan 250100, China*

Xia Gao − *Shandong Agricultural Technology Extending Station, Jinan 250100, China*

Xinyu Liu − *Shandong Provincial Key Laboratory of Applied Mycology, School of Life Sciences, Qingdao Agricultural University, Qingdao 266109, China*

Chenxiao Zhang − *School of Life and Health Sciences, Hainan Province Key Laboratory of One Health, Collaborative Innovation Center of One Health, Hainan University, Haikou 570228, China*

Chunhui Hu − *Shandong Provincial Key Laboratory of Applied Mycology, School of Life Sciences, Qingdao Agricultural University, Qingdao 266109, China*

Lili Xu − *Shandong Provincial Key Laboratory of Applied Mycology, School of Life Sciences, Qingdao Agricultural University, Qingdao 266109, China*

Yanjiao Zhang − *Shandong Provincial Key Laboratory of Applied Mycology, School of Life Sciences, Qingdao Agricultural University, Qingdao 266109, China*

Complete contact information is available at: https://pubs.acs.org/10.1021/acs.jafc.6c05044

Author Contributions

Conceptualization, Hailong Yu, and Hao Yu; Methodology, Xiaohang Li, Hailong Yu, and Hao Yu; Formal analysis, Xiaohang Li, Xianfeng Du, and Chunhui Hu; Investigation, Xiaohang Li, Xianfeng Du, Xinyu Liu, and Chenxiao Zhang; Resources, Lili Xu and Yanjiao Zhang; Software, Xiaohang Li, Xianfeng Du, and Yan Zhang; Data curation, Xiaohang Li and Chunhui Hu; Writing—original draft preparation, Xiaohang Li, Xianfeng Du; Writing—review and editing, Yan Zhang and Hao Yu; Supervision, Xia Gao and Hailong Yu; Project administration, Xia Gao and Hao Yu; Funding acquisition, Xia Gao, Hailong Yu, and Hao Yu; All authors have read and agreed to the published version of the manuscript.

Funding

This study was funded by Key R&D Program of Shandong Province, China (2023LZGCQY013), Chinese National Natural Science Foundation (32272789), Shandong Edible Fungus Agricultural Technology System (SDAIT-07-02), and Sponsored by Experimental Technology Research Programme of Qingdao Agriculture University (SYJS202318).

Notes

The authors declare no competing financial interest.

REFERENCES

(1) Leff, B.; Ramankutty, N.; Foley, J. A. Geographic distribution of major crops across the world. *Global Biogeochem. Cycles* **2004**, *18* (1), 2003GB002108.

(2) Parent, B.; Leclere, M.; Lacube, S.; Semenov, M. A.; Welcker, C.; Martre, P.; Tardieu, F. Maize yields over europe may increase in spite of climate change, with an appropriate use of the genetic variability of flowering time. *Proc. Natl. Acad. Sci. U.S.A.* **2018**, *115* (42), 10642−10647.

(3) Dahmen, N.; Lewandowski, I.; Zibek, S.; Weidtmann, A. Integrated lignocellulosic value chains in a growing bioeconomy: status quo and perspectives. *GCB Bioenergy* **2019**, *11* (1), 107−117.

(4) Jatoi, A. S.; Abbasi, S. A.; Hashmi, Z.; Shah, A. K.; Alam, M. S.; Bhatti, Z. A.; Maitlo, G.; Hussain, S.; Khandro, G. A.; Usto, M. A.; Iqbal, A. Recent trends and future perspectives of lignocellulose biomass for biofuel production: A comprehensive review. *Biomass Convers. Biorefin.* **2023**, *13* (8), 6457−6469.

(5) Taha, M.; Shahsavari, E.; Al-Hothaly, K.; Mouradov, A.; Smith, A. T.; Ball, A. S.; Adetutu, E. M. Enhanced biological straw saccharification through coculturing of lignocellulose-degrading

microorganisms. *Appl. Biochem. Biotechnol.* **2015**, *175* (8), 3709−3728.
(6) Himmel, M. E.; Ding, S.-Y.; Johnson, D. K.; Adney, W. S.; Nimlos, M. R.; Brady, J. W.; Foust, T. D. Biomass recalcitrance: engineering plants and enzymes for biofuels production. *Science* **2007**, *315* (5813), 804−807.
(7) Ragauskas, A. J.; Williams, C. K.; Davison, B. H.; Britovsek, G.; Cairney, J.; Eckert, C. A.; Frederick, W. J.; Hallett, J. P.; Leak, D. J.; Liotta, C. L.; Mielenz, J. R.; Murphy, R.; Templer, R.; Tschaplinski, T. The path forward for biofuels and biomaterials. *Science* **2006**, *311* (5760), 484−489.
(8) Schutyser, W.; Renders, T.; Van Den Bosch, S.; Koelewijn, S.-F.; Beckham, G. T.; Sels, B. F. Chemicals from lignin: an interplay of lignocellulose fractionation, depolymerisation, and upgrading. *Chem. Soc. Rev.* **2018**, *47* (3), 852−908.
(9) Brandt, S. C.; Brognaro, H.; Ali, A.; Ellinger, B.; Maibach, K.; Rühl, M.; Wrenger, C.; Schlüter, H.; Schäfer, W.; Betzel, C.; Janssen, S.; Gand, M. Insights into the genome and secretome of *Fusarium metavorans* DSM105788 by cultivation on agro-residual biomass and synthetic nutrient sources. *Biotechnol. Biofuels* **2021**, *14* (1), 74.
(10) Berovic, M.; Podgornik, B. B.; Gregori, A. Cultivation technologies for production of medicinal mushroom biomass: review. *Int. J. Med. Mushrooms* **2022**, *24* (2), 1−22.
(11) Shevale, S. B.; Deshmukh, H. V. Yield performance and nutritional analysis of Pleurotus species on different agro wastes and vegetable wastes. *Int. J. Plant Prot.* **2016**, *9* (1), 162−167.
(12) Suguimoto, H. H.; Barbosa, A. M.; Dekker, R. F. H.; Castro-Gomez, R. J. H. Veratryl alcohol stimulates fruiting body formation in the oyster mushroom, *Pleurotus ostreatus*. *FEMS Microbiol. Lett.* **2001**, *194* (2), 235−238.
(13) Zhao, Q.; Liu, X.; Cui, L.; Ma, C. Extraction and bioactivities of the chemical composition from *Pleurotus ostreatus*: A Review. *J. Future Foods* **2024**, *4* (2), 111−118.
(14) Yin, Z.; Sun-Waterhouse, D.; Wang, J.; Ma, C.; Waterhouse, G. I. N.; Kang, W. Polysaccharides from edible fungi *Pleurotus* spp.: advances and perspectives. *J. Future Foods* **2021**, *1* (2), 128−140.
(15) Wang, H.; Ma, S.; Mariga, A. M.; Hu, Q.; Xu, Q.; Su, A.; Ma, N.; Ma, G. Structural characterization and anti-Inflammatory activities of novel polysaccharides obtained from *Pleurotus eryngii*. *Food Sci. Hum. Wellness* **2024**, *13* (5), 3031−3042.
(16) Poniedziałek, B.; Mleczek, M.; Niedzielski, P.; Siwulski, M.; Gąsecka, M.; Kozak, L.; Komosa, A.; Rzymski, P. Bio-enriched Pleurotus mushrooms for deficiency control and improved anti-oxidative protection of human platelets? *Eur. Food Res. Technol.* **2017**, *243* (12), 2187−2198.
(17) Siwulski, M.; Mleczek, M.; Rzymski, P.; Budka, A.; Jasińska, A.; Niedzielski, P.; Kalač, P.; Gąsecka, M.; Budzyńska, S.; Mikołajczak, P. Screening the multi-element content of *Pleurotus* mushroom species using inductively coupled plasma optical emission spectrometer (ICP-OES). *Food Anal. Methods* **2017**, *10* (2), 487−496.
(18) Floudas, D.; Binder, M.; Riley, R.; Barry, K.; Blanchette, R. A.; Henrissat, B.; Martínez, A. T.; Otillar, R.; Spatafora, J. W.; Yadav, J. S.; Aerts, A.; Benoit, I.; Boyd, A.; Carlson, A.; Copeland, A.; Coutinho, P. M.; de Vries, R. P.; Ferreira, P.; Findley, K.; Foster, B.; Gaskell, J.; Glotzer, D.; Górecki, P.; Heitman, J.; Hesse, C.; Hori, C.; Igarashi, K.; Jurgens, J. A.; Kallen, N.; Kersten, P.; Kohler, A.; Kües, U.; Kumar, T. K. A.; Kuo, A.; LaButti, K.; Larrondo, L. F.; Lindquist, E.; Ling, A.; Lombard, V.; Lucas, S.; Lundell, T.; Martin, R.; McLaughlin, D. J.; Morgenstern, I.; Morin, E.; Murat, C.; Nagy, L. G.; Nolan, M.; Ohm, R. A.; Patyshakuliyeva, A.; Rokas, A.; Ruiz-Dueñas, F. J.; Sabat, G.; Salamov, A.; Samejima, M.; Schmutz, J.; Slot, J. C.; St John, F.; Stenlid, J.; Sun, H.; Sun, S.; Syed, K.; Tsang, A.; et al. The paleozoic origin of enzymatic mechanisms for lignin degradation reconstructed using 31 fungal genomes. *Science* **2012**, *336* (6089), 1715−1719.
(19) Hage, H.; Miyauchi, S.; Virágh, M.; Drula, E.; Min, B.; Chaduli, D.; Navarro, D.; Favel, A.; Norest, M.; Lesage-Meessen, L.; Bálint, B.; Merényi, Z.; De Eugenio, L.; Morin, E.; Martínez, A. T.; Baldrian, P.; Štursová, M.; Martínez, M. J.; Novotny, C.; Magnuson, J. K.; Spatafora, J. W.; Maurice, S.; Pangilinan, J.; Andreopoulos, W.; LaButti, K.; Hundley, H.; Na, H.; Kuo, A.; Barry, K.; Lipzen, A.; Henrissat, B.; Riley, R.; Ahrendt, S.; Nagy, L. G.; Grigoriev, I. V.; Martin, F.; Rosso, M. Gene family expansions and transcriptome signatures uncover fungal adaptations to wood decay. *Environ. Microbiol.* **2021**, *23* (10), 5716−5732.
(20) Marinovíc, M.; Di Falco, M.; Aguilar Pontes, M. V.; Gorzsás, A.; Tsang, A.; De Vries, R. P.; Mäkelä, M. R.; Hildén, K. Comparative analysis of enzyme production patterns of lignocellulose degradation of two white rot fungi: *Obba rivulosa* and *Gelatoporia subvermispora*. *Biomolecules* **2022**, *12* (8), 1017.
(21) Ruiz-Dueñas, F. J.; Barrasa, J. M.; Sánchez-García, M.; Camarero, S.; Miyauchi, S.; Serrano, A.; Linde, D.; Babiker, R.; Drula, E.; Ayuso-Fernández, I.; Pacheco, R.; Padilla, G.; Ferreira, P.; Barriuso, J.; Kellner, H.; Castanera, R.; Alfaro, M.; Ramírez, L.; Pisabarro, A. G.; Riley, R.; Kuo, A.; Andreopoulos, W.; LaButti, K.; Pangilinan, J.; Tritt, A.; Lipzen, A.; He, G.; Yan, M.; Ng, V.; Grigoriev, I. V.; Cullen, D.; Martin, F.; Rosso, M.-N.; Henrissat, B.; Hibbett, D.; Martínez, A. T. Genomic analysis enlightens agaricales lifestyle evolution and increasing peroxidase diversity. *Mol. Biol. Evol.* **2021**, *38* (4), 1428−1446.
(22) Santoyo, F.; González, A. E.; Terrón, M. C.; Ramírez, L.; Pisabarro, A. G. Quantitative linkage mapping of lignin-degrading enzymatic activities in *Pleurotus ostreatus*. *Enzyme Microb. Technol.* **2008**, *43* (2), 137−143.
(23) Singh, M. P.; Pandey, A. K.; Vishwakarma, S. K.; Srivastava, A. K.; Pandey, V. K.; Agrawal, S.; Singh, V. K. Production of cellulolytic enzymes by *Pleurotus* species on lignocellulosic wastes using novel pretreatments. *Cell. Mol. Biol.* **2014**, *60* (5), 41−45.
(24) Li, Z.; Zhao, C.; Zhou, Y.; Zheng, S.; Hu, Q.; Zou, Y. Label-free comparative proteomic analysis of *Pleurotus eryngii* grown on sawdust, bagasse, and peanut shell substrates. *J. Proteomics* **2024**, *294*, 105074.
(25) Jia, Z.; Wan, X.; Liu, Y.; Lin, C.; Zhang, M.; He, X.; Wang, H.; Du, C.; Li, M.; Qi, J. Multi-Omics integrated analysis provides insights into developmental mechanisms, metabolic variations and key component biosynthesis in the rare medicinal fungus *Gerronema lapidescens*. *Food Biosci.* **2026**, *82*, 109348.
(26) Yu, R.; Zhou, H.; Xiong, M.; Chen, J.; Wang, S.; Xu, W.; Tian, Y.; Su, L. Integrated UHPLC-Q-Exactive-MS/MS metabolomics and network pharmacology to explore the potential mechanism of obesity prevention in *Pleurotus eryngii* treated with different cooking procedures. *J. Future Foods* **2026**, *6* (1), 117−130.
(27) Fernández-Fueyo, E.; Ruiz-Dueñas, F. J.; López-Lucendo, M. F.; Pérez-Boada, M.; Rencoret, J.; Gutiérrez, A.; Pisabarro, A. G.; Ramírez, L.; Martínez, A. T. A secretomic view of woody and nonwoody lignocellulose degradation by *Pleurotus ostreatus*. *Biotechnol. Biofuels* **2016**, *9* (1), 49.
(28) Pell, G.; Taylor, E. J.; Gloster, T. M.; Turkenburg, J. P.; Fontes, C. M. G. A.; Ferreira, L. M. A.; Nagy, T.; Clark, S. J.; Davies, G. J.; Gilbert, H. J. The mechanisms by which family 10 glycoside hydrolases bind decorated substrates. *J. Biol. Chem.* **2004**, *279* (10), 9597−9605.
(29) Pollet, A.; Delcour, J. A.; Courtin, C. M. Structural determinants of the substrate specificities of xylanases from different glycoside hydrolase families. *Crit. Rev. Biotechnol.* **2010**, *30* (3), 176−191.
(30) Fujimoto, Z.; Kishine, N.; Teramoto, K.; Tsutsui, S.; Kaneko, S. Structure-based substrate specificity analysis of GH11 xylanase from *Streptomyces olivaceoviridis* E-86. *Appl. Microbiol. Biotechnol.* **2021**, *105* (5), 1943−1952.
(31) Bajaj, P.; Mahajan, R. Cellulase and xylanase synergism in industrial biotechnology. *Appl. Microbiol. Biotechnol.* **2019**, *103* (21−22), 8711−8724.
(32) Li, X.; Kouzounis, D.; Kabel, M. A.; De Vries, R. P. GH10 and GH11 endoxylanases in *Penicillium subrubescens*: Comparative characterization and synergy with GH51, GH54, GH62 α-l-arabinofuranosidases from the same fungus. *New Biotechnol.* **2022**, *70*, 84−92.
(33) Peña, A.; Babiker, R.; Chaduli, D.; Lipzen, A.; Wang, M.; Chovatia, M.; Rencoret, J.; Marques, G.; Sánchez-Ruiz, M. I.;

https://doi.org/10.1021/acs.jafc.6c05044
J. Agric. Food Chem. XXXX, XXX, XXX−XXX

Kijpornyongpan, T.; Salvachúa, D.; Camarero, S.; Ng, V.; Gutiérrez, A.; Grigoriev, I. V.; Rosso, M.-N.; Martínez, A. T.; Ruiz-Dueñas, F. J. A multiomic approach to understand how *Pleurotus eryngii* transforms non-woody lignocellulosic material. *J. Fungi* **2021**, *7* (6), 426.

(34) Baldrian, P.; Gabriel, J. Lignocellulose degradation by *Pleurotus ostreatus* in the presence of cadmium. *FEMS Microbiol. Lett.* **2003**, *220* (2), 235−240.

(35) Altaf, S. A.; Sughra, M. G.; Nasreen, K.; Umar, D. M.; Sher, M. M.; Noor-e-Saba, K. M.; Fariha, R. K.; Lu, C. Characterization of crude xylanase produced by edible mushroom *Pleurotus eryngii*. *J. Bioprocess. Biotechnol.* **2016**, *6* (2), 6.

(36) Zhu, L.; Ma, S.; Gao, X.; Han, J.; Lu, W.; Yu, H.; Yang, S. Comparative secretome analysis of *Oudemansiella raphanipes* grown on different agricultural residues. *J. Proteomics* **2025**, *317*, 105445.

(37) Li, X.; Chen, X.; Zhao, S.; Jiang, H.; Cai, Y.; Bai, J.; Shao, J.; Yu, H.; Chen, T. Comparative secretome and proteome analysis unveils the response mechanism in the phosphorus utilization of *Alexandrium pacificum*. *Environ. Pollut.* **2025**, *373*, 126135.

(38) Álvarez-Cervantes, J.; Díaz-Godínez, G.; Mercado-Flores, Y.; Gupta, V. K.; Anducho-Reyes, M. A. Phylogenetic analysis of *β*-xylanase srxl1 of *Sporisorium reilianum* and its relationship with families (GH10 and GH11) of Ascomycetes and Basidiomycetes. *Sci. Rep.* **2016**, *6* (1), 24010.

(39) Abramson, J.; Adler, J.; Dunger, J.; Evans, R.; Green, T.; Pritzel, A.; Ronneberger, O.; Willmore, L.; Ballard, A. J.; Bambrick, J.; Bodenstein, S. W.; Evans, D. A.; Hung, C.-C.; O'Neill, M.; Reiman, D.; Tunyasuvunakool, K.; Wu, Z.; Žemgulytė, A.; Arvaniti, E.; Beattie, C.; Bertolli, O.; Bridgland, A.; Cherepanov, A.; Congreve, M.; Cowen-Rivers, A. I.; Cowie, A.; Figurnov, M.; Fuchs, F. B.; Gladman, H.; Jain, R.; Khan, Y. A.; Low, C. M. R.; Perlin, K.; Potapenko, A.; Savy, P.; Singh, S.; Stecula, A.; Thillaisundaram, A.; Tong, C.; Yakneen, S.; Zhong, E. D.; Zielinski, M.; Žídek, A.; Bapst, V.; Kohli, P.; Jaderberg, M.; Hassabis, D.; Jumper, J. M. Accurate structure prediction of biomolecular interactions with AlphaFold 3. *Nature* **2024**, *630* (8016), 493−500.

(40) Eberhardt, J.; Santos-Martins, D.; Tillack, A. F.; Forli, S. AutoDock Vina 1.2.0: new docking methods, expanded force field, and python bindings. *J. Chem. Inf. Model.* **2021**, *61* (8), 3891−3898.

(41) Chen, M.; Li, Q.; Liu, C.; Meng, E.; Zhang, B. Microbial degradation of lignocellulose for sustainable biomass utilization and future research perspectives. *Sustainability* **2025**, *17* (9), 4223.

(42) Melanouri, E.-M.; Dedousi, M.; Diamantopoulou, P. Cultivating *Pleurotus ostreatus* and *Pleurotus eryngii* mushroom strains on agro-industrial residues in solid-state fermentation. part I: Screening for growth, endoglucanase, laccase and biomass production in the colonization phase. *Carbon Resour. Convers.* **2022**, *5* (1), 61−70.

(43) Elisashvili, V.; Metreveli, E.; Khardziani, T.; Sokhadze, K.; Kobakhidze, A.; Kachlishvili, E. Review of recent advances in the physiology of the regulation of cellulase and xylanase production by Basidiomycetes. *Energies* **2023**, *16* (11), 4382.

(44) Stricker, A. R.; Grosstessner-Hain, K.; Würleitner, E.; Mach, R. L. Xyr1 (xylanase regulator 1) regulates both the hydrolytic enzyme system and d -xylose metabolism in Hypocrea jecorina. *Eukaryot. Cell* **2006**, *5* (12), 2128−2137.

(45) Van Den Brink, J.; De Vries, R. P. Fungal enzyme sets for plant polysaccharide degradation. *Appl. Microbiol. Biotechnol.* **2011**, *91* (6), 1477−1492.

(46) Andlar, M.; Rezić, T.; Marđetko, N.; Kracher, D.; Ludwig, R.; Šantek, B. Lignocellulose degradation: An overview of fungi and fungal enzymes involved in lignocellulose degradation. *Eng. Life Sci.* **2018**, *18* (11), 768−778.

(47) Chen, L.; Gong, Y.; Cai, Y.; Liu, W.; Zhou, Y.; Xiao, Y.; Xu, Z.; Liu, Y.; Lei, X.; Wang, G.; Guo, M.; Ma, X.; Bian, Y. Genome sequence of the edible cultivated mushroom *Lentinula edodes* (shiitake) reveals insights into lignocellulose degradation. *PLoS One* **2016**, *11* (8), No. e0160336.

(48) Ramoni, J.; Marchetti-Deschmann, M.; Seidl-Seiboth, V.; Seiboth, B. *Trichoderma reesei* xylanase 5 is defective in the reference strain QM6a but functional alleles are present in other wild-type strains. *Appl. Microbiol. Biotechnol.* **2017**, *101* (10), 4139−4149.

(49) Zhang, S.; Zhao, S.; Shang, W.; Yan, Z.; Wu, X.; Li, Y.; Chen, G.; Liu, X.; Wang, L. Synergistic mechanism of GH11 xylanases with different action modes from *Aspergillus niger* An76. *Biotechnol. Biofuels* **2021**, *14* (1), 118.

(50) Sapag, A.; Wouters, J.; Lambert, C.; De Ioannes, P.; Eyzaguirre, J.; Depiereux, E. The endoxylanases from family 11: computer analysis of protein sequences reveals important structural and phylogenetic relationships. *J. Biotechnol.* **2002**, *95* (2), 109−131.

(51) Wakarchuk, W. W.; Campbell, R. L.; Davoodi, J.; Yaguchi, M. Mutational and crystallographic analyses of the active site residues of the *Bacillus circulans* xylanase. *Protein Sci.* **1994**, *3* (3), 467−475.

(52) Yu, H.; Zhao, S.; Fan, Y.; Hu, C.; Lu, W.; Guo, L. Cloning and heterologous expression of a novel halo/alkali-stable multi-domain xylanase ($XylM_{18}$) from a marine bacterium *Marinimicrobium* sp. strain LS-A18. *Appl. Microbiol. Biotechnol.* **2019**, *103* (21−22), 8899−8909.

(53) Black, G. W.; Rixon, J. E.; Clarke, J. H.; Hazlewood, G. P.; Theodorou, M. K.; Morris, P.; Gilbert, H. J. Evidence that linker sequences and cellulose-binding domains enhance the activity of hemicellulases against complex substrates. *Biochem. J.* **1996**, *319* (2), 515−520.

(54) McLean, B. W.; Bray, M. R.; Boraston, A. B.; Gilkes, N. R.; Haynes, C. A.; Kilburn, D. G. Analysis of binding of the family 2a carbohydrate-binding module from *Cellulomonas fimi* xylanase 10A to cellulose: specificity and identification of functionally important amino acid residues. *Protein Eng.* **2000**, *13* (11), 801−809.

(55) Inoue, H.; Kishishita, S.; Kumagai, A.; Kataoka, M.; Fujii, T.; Ishikawa, K. Contribution of a family 1 carbohydrate-binding module in thermostable glycoside hydrolase 10 xylanase from *Talaromyces cellulolyticus* toward synergistic enzymatic hydrolysis of lignocellulose. *Biotechnol. Biofuels* **2015**, *8* (1), 77.

(56) Miao, Y.; Kong, Y.; Li, P.; Li, G.; Liu, D.; Shen, Q.; Zhang, R. Effect of CBM1 and linker region on enzymatic properties of a novel thermostable dimeric GH10 xylanase (Xyn10A) from filamentous fungus *Aspergillus fumigatus* Z5. *AMB Expr* **2018**, *8* (1), 44.

(57) Shibata, N.; Suetsugu, M.; Kakeshita, H.; Igarashi, K.; Hagihara, H.; Takimura, Y. A novel GH10 xylanase from *Penicillium* sp. accelerates saccharification of alkaline-pretreated bagasse by an enzyme from recombinant *Trichoderma reesei* expressing *Aspergillus β*-glucosidase. *Biotechnol. Biofuels* **2017**, *10* (1), 278.

(58) Liu, S.; Ding, S. Replacement of carbohydrate binding modules improves acetyl xylan esterase activity and its synergistic hydrolysis of different substrates with xylanase. *BMC Biotechnol.* **2016**, *16* (1), 73.

(59) Liu, C.; Zhang, Y.; Ye, C.; Zhao, F.; Chen, Y.; Han, S. Combined strategies for improving the heterologous expression of a novel xylanase from *Fusarium oxysporum* Fo47 in *Pichia pastoris*. *Synth. Syst. Biotechnol.* **2024**, *9* (3), 426−435.

(60) Rodríguez, S.; González, C.; Reyes-Godoy, J. P.; Gasser, B.; Andrews, B.; Asenjo, J. A. Expression and characterization of cold-adapted xylanase Xyl-L in *Pichia pastoris* for xylooligosaccharide (XOS) preparation. *Microb. Cell Fact.* **2025**, *24* (1), 82.

(61) Mishra, C.; Forrester, I. T.; Kelley, B. D.; Burgess, R. R.; Leatham, G. F. Characterization of a major xylanase purified from *Lentinula edodes* cultures grown on a commercial solid lignocellulosic substrate. *Appl. Microbiol. Biotechnol.* **1990**, *33* (2), 226−232.

(62) Gao, M.; Shi, Z. Process control and optimization for heterologous protein production by methylotrophic *Pichia pastoris*. *Chin. J. Chem. Eng.* **2013**, *21* (2), 216−226.

(63) Lin-Cereghino, G. P.; Godfrey, L.; De La Cruz, B. J.; Johnson, S.; Khuongsathiene, S.; Tolstorukov, I.; Yan, M.; Lin-Cereghino, J.; Veenhuis, M.; Subramani, S.; Cregg, J. M. Mxr1p, a key regulator of the methanol utilization pathway and peroxisomal genes in *Pichia pastoris*. *Mol. Cell. Biol.* **2006**, *26* (3), 883−897.

(64) Bhardwaj, N.; Kumar, B.; Verma, P. A detailed overview of xylanases: an emerging biomolecule for current and future prospective. *Bioresour. Bioprocess.* **2019**, *6* (1), 40.

https://doi.org/10.1021/acs.jafc.6c05044
J. Agric. Food Chem. XXXX, XXX, XXX−XXX

(65) Lee, C. C.; Wong, D. W. S.; Robertson, G. H. Cloning and characterization of the xyn11A gene from *Lentinula edodes*. *Protein J.* **2005**, *24* (1), 21−26.
(66) Le, Y.; Wang, H. High-level soluble expression of a thermostable xylanase from thermophilic fungus *Thermomyces lanuginosus* in *Escherichia coli* via fusion with OsmY protein. *Protein Expr. Purif.* **2014**, *99*, 1−5.
(67) Li, L.; Qu, M.; Liu, C.; Xu, L.; Pan, K.; Song, X.; OuYang, K.; Li, Y.; Zhao, X. Expression of a recombinant *Lentinula edodes* xylanase by *Pichia pastoris* and its effects on ruminal fermentation and microbial community in in vitro incubation of agricultural straws. *Front. Microbiol.* **2018**, *9*, 2944.
(68) Waris, A.; Awan, A. R.; Wasim, M.; Hashmi, A. S.; Rashid, N.; Firyal, S.; Khalid, A.; Tayyab, M. 3D modeling of thermostable xylanase from *Thermotoga naphthophila* a member of GH10 family: characterization studies of recombinant xylanase. *bioRxiv* **2024**, 09.06.611769.
(69) Akyol, I.; Comlekcioglu, U.; Kar, B.; Ekinci, M. S.; Ozkose, E. Cloning of a xylanase gene xyn2A from rumen fungus *Neocallimastix* sp. GMLF2 in *Escherichia coli* and its partial characterization. *Biologia* **2009**, *64* (4), 664−670.
(70) Li, J.-F.; Gao, S.-J.; Liu, X.-T.; Gong, Y.-Y.; Chen, Z.-F.; Wei, X.-H.; Zhang, H.-M.; Wu, M.-C. Modified pPIC9K vector-mediated expression of a family 11 xylanase gene, Aoxyn11A, from *Aspergillus oryzae* in *Pichia pastoris*. *Ann. Microbiol.* **2013**, *63* (3), 1109−1120.
(71) Ouephanit, C.; Boonvitthya, N.; Bozonnet, S.; Chulalaksananukul, W. High-level heterologous expression of endo-1,4-β-xylanase from *Penicillium citrinum* in *Pichia pastoris* X-33 directed through codon optimization and optimized expression. *Molecules* **2019**, *24* (19), 3515.
(72) Sanghi, A.; Garg, N.; Gupta, V. K.; Mittal, A.; Kuhad, R. C. One-step purification and characterization of cellulase-free xylanase produced by alkalophilic *Bacillus subtilis* ash. *Braz. J. Microbiol.* **2010**, *41* (2), 467−476.
(73) Guo, B.; Li, P.-Y.; Yue, Y.-S.; Zhao, H.-L.; Dong, S.; Song, X.-Y.; Sun, C.-Y.; Zhang, W.-X.; Chen, X.-L.; Zhang, X.-Y.; Zhou, B.-C.; Zhang, Y.-Z. Gene cloning, expression and characterization of a novel xylanase from the marine bacterium, *Glaciecola mesophila* KMM241. *Mar. Drugs* **2013**, *11* (4), 1173−1187.
(74) Kumar, P. Isolation, purification and characterization of xylanase produced by fish gut *Bacillus cereus* through submerged fermentation. *J. Exp. Zool.* **2023**, *26* (2), 2319−2327.
(75) Zhang, X.; Liu, H.; Ju, L.; Liu, C. Exploring the effect of Cu^{2+} on sludge hydrolysis and interaction mechanism between Cu^{2+} and xylanase by multispectral and thermodynamic methods. *Water, Air, Soil Pollut.* **2017**, *228* (3), 99.
(76) Badon, M. M.; Tekverk, D. G.; Vishnosky, N. S.; Woolridge, E. M. Establishing the oxidative tolerance of *Thermomyces lanuginosus* xylanase. *J. Appl. Microbiol.* **2019**, *127* (2), 508−519.
(77) He, L.; Yan, M.; Naeem, M.; Chen, M.; Chen, Y.; Ni, Z.; Chen, H. Enhancing manganese peroxidase: innovations in genetic modification, screening processes, and sustainable agricultural applications. *J. Agric. Food Chem.* **2024**, *72* (47), 26040−26056.
(78) Molinelli, L.; Drula, E.; Gaillard, J.-C.; Navarro, D.; Armengaud, J.; Berrin, J.-G.; Tron, T.; Tarrago, L. Methionine oxidation of carbohydrate-active enzymes during white-rot wood decay. *Appl. Environ. Microbiol.* **2024**, No. e01931−23.
(79) Hori, C.; Gaskell, J.; Igarashi, K.; Kersten, P.; Mozuch, M.; Samejima, M.; Cullen, D. Temporal alterations in the secretome of the selective ligninolytic fungus *Ceriporiopsis subvermispora* during growth on aspen wood reveal this organism's strategy for degrading lignocellulose. *Appl. Environ. Microbiol.* **2014**, *80* (7), 2062−2070.
(80) Sugumaran, K. R.; Srivastava, S. N.; Ponnusami, V. Kinetic and thermodynamic characterization of *Pleurotus eryngii* MTCC 1798 xylanase and *Fusarium oxysporum* MTCC3300 xylanase: A comparision. *Int. J. Chem. Sci.* **2012**, *10* (3), 1626−1636.
(81) Mukherjee, M.; Sengupta, S. An Inducible Xylanase of the mushroom *Termitomyces clypeatus* differing from the xylanase/amylase produced in dextrin medium. *Microbiology* **1985**, *131* (8), 1881−1885.
(82) Liao, H.; Zheng, H.; Li, S.; Wei, Z.; Mei, X.; Ma, H.; Shen, Q.; Xu, Y. Functional diversity and properties of multiple xylanases from *Penicillium oxalicum* GZ-2. *Sci. Rep.* **2015**, *5* (1), 12631.
(83) Heinen, P. R.; Bauermeister, A.; Ribeiro, L. F.; Messias, J. M.; Almeida, P. Z.; Moraes, L. A. B.; Vargas-Rechia, C. G.; De Oliveira, A. H. C.; Ward, R. J.; Filho, E. X. F.; Kadowaki, M. K.; Jorge, J. A.; Polizeli, M. L. T. M. GH11 xylanase from *Aspergillus tamarii* kita: Purification by one-step chromatography and xylooligosaccharides hydrolysis monitored in real-time by mass spectrometry. *Int. J. Biol. Macromol.* **2018**, *108*, 291−299.
(84) Riadi, L.; Agustin, Y. E.; Ong, L. K.; Hadiwijaya, F. A.; Winoto, A.; Gunawan, E. A.; Tambatjong, J.; Kok, T. Performance and kinetic study of xylan hydrolysis by free and immobilized *Trichoderma* xylanase. In *Proceedings of the 4th International Conference on Informatics, Technology and Engineering 2023 (InCITE 2023)*; Atlantis Highlights in Engineering, 2023; Vol. *21*, pp 62−68; Dordrecht.
(85) Modenbach, A. A.; Nokes, S. E. Enzymatic hydrolysis of biomass at high-solids loadings − a review. *Biomass Bioenergy* **2013**, *56*, 526−544.
(86) Cornish-Bowden, A. *Fundamentals of Enzyme Kinetics*; Butterworths: London ; Boston, 1979.
(87) Yin, E.; Le, Y.; Pei, J.; Shao, W.; Yang, Q. High-level expression of the xylanase from Thermomyces lanuginosus in *Escherichia coli*. *World J. Microbiol. Biotechnol.* **2008**, *24* (2), 275−280.
(88) Singh, R. K.; Tiwari, M. K.; Kim, D.; Kang, Y. C.; Ramachandran, P.; Lee, J.-K. Molecular cloning and characterization of a GH11 endoxylanase from *Chaetomium globosum*, and its use in enzymatic pretreatment of biomass. *Appl. Microbiol. Biotechnol.* **2013**, *97* (16), 7205−7214.
(89) Meng, D.-D.; Ying, Y.; Chen, X.-H.; Lu, M.; Ning, K.; Wang, L.-S.; Li, F.-L. Distinct roles for carbohydrate-binding modules of glycoside hydrolase 10 (GH10) and GH11 xylanases from *Caldicellulosiruptor* sp. strain F32 in thermostability and catalytic efficiency. *Appl. Environ. Microbiol.* **2015**, *81* (6), 2006−2014.
(90) Hervé, C.; Rogowski, A.; Blake, A. W.; Marcus, S. E.; Gilbert, H. J.; Knox, J. P. Carbohydrate-binding modules promote the enzymatic deconstruction of intact plant cell walls by targeting and proximity effects. *Proc. Natl. Acad. Sci. U.S.A.* **2010**, *107* (34), 15293−15298.
(91) Cervera Tison, M.; André-Leroux, G.; Lafond, M.; Georis, J.; Juge, N.; Berrin, J.-G. Molecular determinants of substrate and inhibitor specificities of the *Penicillium griseofulvum* family 11 xylanases. *Biochim. Biophys. Acta Proteins Proteom.* **2009**, *1794* (3), 438−445.
(92) Wan, Q.; Zhang, Q.; Hamilton-Brehm, S.; Weiss, K.; Mustyakimov, M.; Coates, L.; Langan, P.; Graham, D.; Kovalevsky, A. X-ray crystallographic studies of family 11 xylanase Michaelis and product complexes: implications for the catalytic mechanism. *Acta Crystallogr. D Biol. Crystallogr.* **2014**, *70* (1), 11−23.
(93) Boraston, A. B.; Bolam, D. N.; Gilbert, H. J.; Davies, G. J. Carbohydrate-binding modules: fine-tuning polysaccharide recognition. *Biochem. J.* **2004**, *382* (3), 769−781.
(94) Wu, X.; Zhang, S.; Zhang, Q.; Zhao, Y.; Chen, G.; Guo, W.; Wang, L. The contribution of specific subsites to catalytic activities in active site architecture of a GH11 xylanase. *Appl. Microbiol. Biotechnol.* **2020**, *104* (20), 8735−8745.
(95) Alcobaça, O. S. A.; Campanini, E. B.; Ciancaglini, I.; Rocha, S. V.; Malavazi, I.; Freire, C. C. M.; Nunes, F. M. F.; Fuentes, A. S. C.; Cunha, A. F. Identification of a new endo-β-1,4-xylanase prospected from the microbiota of the termite *Heterotermes tenuis*. *Microorganisms* **2022**, *10* (5), 906.
(96) Sarangi, A.; Behera, S.; Paul, M.; Sahu, S. K.; Kumar, R.; Thatoi, H. Structural and functional insights from molecular modeling, docking, and md simulations of bacterial xylanase: implications for biofuel efficiency. *Syst. Microbiol. Biomanuf.* **2025**, *5* (3), 1191−1210.
(97) Mao, M.; Ahrens, L.; Luka, J.; Contreras, F.; Kurkina, T.; Bienstein, M.; Sária Pereira De Passos, M.; Schirinzi, G.; Mehn, D.;

https://doi.org/10.1021/acs.jafc.6c05044
J. Agric. Food Chem. XXXX, XXX, XXX−XXX

Valsesia, A.; Desmet, C.; Serra, M.-A.; Gilliland, D.; Schwaneberg, U. Material-specific binding peptides empower sustainable innovations in plant health, biocatalysis, medicine and microplastic quantification. *Chem. Soc. Rev.* **2024**, *53* (12), 6445−6510.
(98) Jia, H.; Feng, X.; Huang, J.; Guo, Y.; Zhang, D.; Li, X.; Zhao, J. Recombinant family 1 carbohydrate-binding modules derived from fungal cellulase enhance enzymatic degradation of lignocellulose as novel effective accessory protein. *Front. Microbiol.* **2022**, *13*, 876466.
(99) Yang, Y.; Zhang, C.; Lu, H.; Wu, Q.; Wu, Y.; Li, W.; Li, X. Improvement of thermostability and catalytic efficiency of xylanase from *Myceliophthora thermophilar* by N-terminal and C-terminal truncation. *Front. Microbiol.* **2024**, *15*, 1385329.
(100) Ma, J.; Sun, Z.; Ni, Z.; Qi, Y.; Sun, Q.; Hu, Y.; Li, C. Molecular identification and engineering a salt-tolerant GH11 xylanase for efficient xylooligosaccharides production. *Biomolecules* **2024**, *14* (9), 1188.
(101) Miao, H.; Ma, Y.; Zhe, Y.; Tang, X.; Wu, Q.; Huang, Z.; Han, N. Improving the thermostability of a fungal GH11 xylanase via fusion of a submodule (C2) from hyperthermophilic CBM9_1−2. *Int. J. Mol. Sci.* **2022**, *23* (1), 463.
(102) Wang, D.; Wu, J.; Du, J.; Xu, X.; Jiang, S.; Wang, Y.; Li, T.; Wang, Y.; Li, T.; Li, C.; Zhou, C. Thermostability enhancement of the GH11 xylanase XynZT-1 from *Alteromonas macleodii* HY35 achieved via modular mosaic engineering. *J. Agric. Food Chem.* **2025**, *73* (52), 33141−33155.

https://doi.org/10.1021/acs.jafc.6c05044
J. Agric. Food Chem. XXXX, XXX, XXX−XXX